

## **A Population-Average MRI-Based Atlas Collection of the Rhesus Macaque**

Running title: Macaque Atlas

Donald G. McLaren<sup>1,2,3</sup>, Kristopher J. Kosmatka<sup>1,3</sup>, Terrance R. Oakes<sup>8</sup>,  
Christopher D. Kroenke<sup>4,5</sup>, Steven G. Kohama<sup>5</sup>, John A. Matochik<sup>6</sup>, Don K.  
Ingram<sup>7</sup> and Sterling C. Johnson<sup>1,3</sup>

<sup>1</sup>Geriatric Research Education and Clinical Center, Wm. S. Middleton Memorial Veterans Hospital, Madison, WI 53705, USA

<sup>2</sup>Neuroscience Training Program, University of Wisconsin, Madison, WI 53706, USA

<sup>3</sup>Department of Medicine, University of Wisconsin, Madison, WI, 53705 USA

<sup>4</sup>Advanced Imaging Research Center, Oregon Health and Science University, Portland, OR 97239, USA

<sup>5</sup>Division of Neuroscience, Oregon National Primate Research Center, Oregon Health and Science University, Beaverton, OR 97006, USA

<sup>6</sup>Neuroimaging Research Branch, Intramural Research Program, National Institute on Drug Abuse, Baltimore, MD 21224, USA

<sup>7</sup>Nutritional Neuroscience and Aging Laboratory, Pennington Biomedical Research Center, Louisiana State University System, Baton Rouge, LA 70808, USA

<sup>8</sup>Waisman Center Brain Imaging Laboratory, University of Wisconsin, Madison, WI 53705, USA.

**Abstract**

Magnetic resonance imaging (MRI) studies of non-human primates are becoming increasingly common; however, the well-developed voxel-based methodologies used in human studies are not readily applied to non-human primates. In the present study, we create a population-average MRI-based atlas collection for the rhesus macaque (*Macaca mulatta*) that can be used with common brain mapping packages such as SPM or FSL. In addition to creating a publicly available T1-weighted atlas (<http://www.brainmap.wisc.edu/monkey.html>), probabilistic tissue classification maps and T2-weighted atlases were also created. These atlases are aligned to the MRI volume from the Saleem-Logothetis (2006) atlas providing an explicit link to histological sections. Additionally, we have created a transform to integrate these atlases with the F99 surface-based atlas in CARET. It is anticipated that these tools will help facilitate voxel-based imaging methodologies in non-human primate species, which in turn may increase our understanding of brain function, development, and evolution.

## Introduction

Functional and structural neuroimaging research studies in humans have benefited greatly from rapidly maturing computational neuroanatomical methods that enable multi-subject voxel-wise approaches (Ashburner and Friston, 2000; Friston et al., 1999a; Friston et al., 1999b; Woods, 1996). The first major advance in multi-subject analyses was the advent of objective normalization procedures for PET imaging (Fox et al., 1985). Fox and colleagues developed a stereotaxic transforms for individual subjects to a common reference space, which was the first objective approach used to normalize subjects (Fox et al., 1985). Importantly, this method enabled the use of a common atlas space and improved power by allowing the analyses across subjects. Another critical advance was the development of imaging atlases in a standard coordinate space (e.g. MNI152) created from many individuals (Evans et al., 1993; Evans et al., 1994; Mazziotta et al., 2001; Mazziotta et al., 1995). The standardized atlas serves as a target space to which any individual brain can be spatially normalized, and provides a standard coordinate system to report results and thereby enhance comparisons and generalizability across labs. Such approaches are now the standard in human brain mapping methodologies including functional imaging with fMRI and PET using voxel-based (Ashburner et al., 1998; Woods et al., 1999; Woods et al., 1998a; Woods et al., 1998b; Zeffiro et al., 1997) and surface-based (Fischl et al., 1999; Van Essen, 2005) methods (though different standard atlas spaces exist -- see Devlin and Poldrack, 2007).

Accessible population-average atlases in a standard coordinate space for non-human primate (NHP) species, such as rhesus macaque (*Macaca mulatta*), are less common. Although atlases exist for the rhesus macaque, they are based on post-mortem slices (Martin and Bowden, 1996; Mikula et al., 2007; Paxinos, 2000) and thus do not provide an accessible MRI target to which individual animals can be spatially normalized. Furthermore, atlases are typically based on a single subject and are thus less likely to be representative of the population.

There are currently a handful of NHP atlases available to the imaging community. Most of these atlases are based on a single animal (Cannestra et al., 1997; Saleem and Logothetis, 2006; Van Essen, 2002, 2004); while others are based on small samples of 6-12 animals (Black et al., 2001a; Black et al., 2001b; Greer et al., 2002; Vincent et al., 2007). NHP atlases that are based on multiple animals capture more of the variability in the species from which they were drawn, and for this reason may be preferable to single-subject atlases. However, due to inter-species variability, NHP atlases should be species-specific. Examples of species-specific non-human primate multi-subject, population-average atlases include *Macaca nemestrina* (Black et al., 2001a; see -- <http://www.nil.wustl.edu/labs/kevin/ni/n2k/> and [http://www.ioni.ucla.edu/Atlases/Atlas\\_Detail.jsp?atlas\\_id=2](http://www.ioni.ucla.edu/Atlases/Atlas_Detail.jsp?atlas_id=2); 2004), *Macaca fascicularis* (Vincent et al., 2007; also see -- <http://www.nil.wustl.edu/labs/kevin/ni/cyno/cyno.html>), *Papio anubis* (Black et al., 2001b; see -- <http://www.nil.wustl.edu/labs/kevin/ni/b2k/>; Greer et al., 2002). Black and colleagues studied nine *Papio anubis* to create the first probabilistic

NHP atlas. Briefly, their method aligned their baboons to the Davis and Huffman atlas (Davis and Huffman, 1968), averaged them together to create an initial average, aligned the average to the atlas, and then aligned their baboons to the initial average, averaged the individuals again, and aligned the average to the Davis and Huffman atlas with 20 iterations (Black et al., 1997; Black et al., 2001b).

The rhesus macaque is a very commonly studied NHP species for which a population-average atlas does not exist; the development for such an atlas is the focus of this report. This atlas is based on the coordinate space of the single-subject atlas of Saleem-Logothetis (D99-SL) which includes MRI sections coregistered to histological slices (nissl, parvalbumin, SMI-32, calbindin and calretinin) and cytoarchitectonic areas (Saleem and Logothetis, 2006). We created a T1-weighted population-average template in the space of D99-SL. In addition, we present probabilistic tissue classification maps, prior probability maps, that can improve tissue segmentation in NHP MR images and illustrate their application. We also created T2-weighted atlas to complement the T1-weighted volume atlas. Finally, we created a transform to the F99 surface-based atlas to facilitate comparisons with other primate species (e.g. humans and fascicularis macaques, see --Van Essen and Dierker, 2007).

## **Materials and Methods**

Eighty-two male and thirty female rhesus macaques (*Macaca mulatta*) underwent MR imaging at one of three imaging sites. Rhesus macaque

demographics are detailed in Table I. All monkeys belonged to existing primate colonies at one of three sites: the National Institutes of Health Animal Center (NIHAC) in Poolesville, MD, USA; the Oregon National Primate Research Center at the Oregon Health and Science University (ONPRC/OHSU) in Beaverton, OR, USA; the Wisconsin National Primate Research Center at the University of Wisconsin – Madison (WNPRC/UW), Madison, WI, USA. All facilities are fully accredited by the Association for Assessment and Accreditation of Laboratory Animal Care. Additionally, the research protocols were approved by the Institutional Animal Care and Use Committee of the Gerontology Research Center, NIA; the Institutional Animal Care and Use Committee at ONPRC, OHSU; and the Research Animal Resources Center at the University of Wisconsin, UW; respectively.

#### *UW Image Acquisition*

Images were acquired on a General Electric 3.0 T Signa MR unit (GE Medical Systems, Milwaukee, WI, USA) using a quadrature Tx/Rx volume coil with an 18 cm diameter at the Waisman Center for Brain Imaging and Behavior on the medical campus of the University of Wisconsin, Madison, WI, USA. During the scanning procedure, the monkeys were anesthetized with ketamine (up to 15 mg/kg [100 mg/ml], IM) or alternative anesthesia in consultation with WNPRC veterinarian and xylazine (up to 0.6 mg/kg [20 mg/ml], IM). Occasionally, animals were resedated during the scan with additional ketamine HCl (7-15 mg/kg [100 mg/ml], IM or IV) with or without xylazine (0.2-0.6 mg/kg [20 mg/ml], IM or IV). A

three-dimensional coronal T1-weighted inversion recovery-prepped spoiled gradient echo (IR-prepped SPGR) with the following parameters: TR, 8.772 ms; TE, 1.876 ms; TI, 600 ms; FA, 10°; NEX, 2; acquisition matrix, 256x256; FOV, 160 mm. 124 coronal slices with a thickness of 0.7 mm were acquired. These parameters resulted in 0.6 x 0.6 x 0.7 mm voxels. A T2-weighted extended echo train acquisition (XETA) (Busse et al., 2006; Gold et al., 2007) scan was acquired in nine of these monkeys with the following parameters: TR, 2300 ms; TE, 81.56 ms; FA, 55°; NEX, .547; acquisition matrix, 256x256 (resampled to 512x512); FOV, 140 mm; 248 sagittal overlapping 0.8 mm thick slices; resulting voxel size, 0.27 x 0.27 x 0.4 mm.

### *OHSU Image Acquisition*

Images were acquired on a Siemens 3.0 T Trio MR unit (Erlangen, Germany) using a Siemens circularly-polarized knee “extremity” (EX) coil for RF transmission and reception at the Advanced Imaging Research Center, located on the main campus of OHSU in Portland, OR, USA. Animals were transported to the MRI unit in transfer cages and were anesthetized with ketamine HCl (10 mg/kg body weight, im), intubated, then maintained on 1% isoflurane vaporized in oxygen for the duration of the scan. A three-dimensional coronal T1-weighted magnetization prepared rapid gradient echo (MPRAGE) with the following parameters: TR, 2500 ms; TE, 4.38 ms; inversion time [TI], 1100 ms; FA, 12°; NEX, 1; acquisition matrix, 256x256; FOV, 120 mm. 88 coronal slices with a

thickness of 1 mm were acquired. These parameters resulted in 0.46875 x 0.46875 x 1.0 mm voxels.

### *NIA Image Acquisition*

Images were acquired on a General Electric 1.5 T Signa MR unit (GE Medical Systems, Milwaukee, WI, USA) using a surface coil at the NIH MRI Research Facility in Bethesda, MD, USA. During the scanning procedure, the monkeys were anesthetized with 6 mg/kg i.m. of telazol (Aveco, Fort Dodge, IA, USA) and 0.05–0.1 mg/kg i.m. of acepromazine (Ayerst, New York, NY, USA). A three-dimensional transaxial T1-weighted spoiled gradient echo (SPGR) with the following parameters: repetition time [TR], 15.2 ms; echo time [TE], 6.1 ms; flip angle [FA], 30°; number of excitations [NEX], 2; acquisition matrix, 256x256; field of view [FOV], 100 mm. 124 transaxial slices with a thickness of 1mm were acquired and resampled to 0.39mm. These parameters resulted in 0.39 x 0.39 x 0.39 mm voxels.

### *T1-Weighted Volume Atlas Creation*

Volume atlas creation used the following semi-automated approach (Figure 1) similar to that used by Black and colleagues in other non-human primate species (Black et al., 1997; Black et al., 2001a, 2004; Black et al., 2001b). First, raw scanner images are reconstructed to form 3D volumes for each individual monkey. Next, 3D object maps were manually drawn by trained individuals to delineate brain from non-brain tissues using ANALYZE (Mayo

Clinic, Rochester, MN; see -- Robb, 2001). The object maps excluded the optic tract anterior to the optic chiasm and brainstem inferior to the pons. Binary mask volumes derived from the object maps were used to extract corresponding voxels from the original MRI volumes to create deskulled brain volumes. The deskulled and original volumes were manually rotated to match the left, posterior, inferior orientation of the D99-SL volume (Saleem and Logothetis, 2006). Subsequently, each deskulled volume entered the following supervised, but automated procedure: (i) bias corrected for field inhomogeneity using “fast” algorithm in FSL (FMRIB Analysis Group, University of Oxford, UK) which also provides segmentation maps (Zhang et al., 2001); and (ii) intensity normalization by scaling the mean white matter intensity (mean voxel value within white matter segment created in the prior step) to 300. Following these two processing steps, atlas creation was achieved through the following iterative process: (i) registered to the target volume using a 12 parameter affine transformation (Jenkinson and Smith, 2001); (ii) averaged the registered brain volumes together; and (iii) registered the averaged volume to the D99-SL volume to ensure accurate coregistration between the average and the published atlas. The first iteration used D99-SL volume (Saleem and Logothetis, 2006) as the target to create an initial template. In the second iteration, the process was repeated using the initial template as the target. The stereotaxic space and orientation (left, posterior, inferior) of the D99-SL atlas are retained (Saleem and Logothetis, 2006). Thus, the 112RM-SL atlas (Figure 2) has the same origin as the D99-SL atlas which was set to “Ear Bar Zero” – the rostrocaudal reference is the vertical plane

passing through the interaural line, the dorsoventral reference is the horizontal plane passing through the interaural line, the left-right reference is the vertical plane passing through the midline (Saleem and Logothetis, 2006).

### *T2-Weighted Volume Atlas Creation*

Nine rhesus macaques were used to create a T2-weighted atlas using the following steps: (i) selected one T2-weighted scan and registered it to the T1-weighted atlas using a 12 parameter affine transformation; (ii) all images then entered into the processing stream described in the T1-weighted atlas creation except the registered T2-weighted image replaced the D99-SL target in the first iteration; (iii) after the second iteration the T2-weighted atlas was registered to the T1-weighted atlas using a 12 parameter affine transformation to ensure the two atlases are aligned (Figure 2).

### *Prior Probability Maps*

Probabilistic tissue classification maps, prior probability maps, with .5 mm isotropic voxels were created using existing methods (Evans et al., 1993; Evans et al., 1994; Kamber et al., 1992). Due to contrast differences between cohorts (Figure S1), only animals from the OHSU and UW cohorts were used for the probability maps. First, the aforementioned deskulled volumes were registered to the combined-SL atlas using a 12 parameter affine transformation (Jenkinson and Smith, 2001). Next, the registered volumes were segmented using “fast” in FSL, which performs an integrated bias correction and segmentation procedure

(Zhang et al., 2001). The outputs of “fast” were binary coded segmentation images for each tissue class (gray matter, white matter, and cerebral spinal fluid). Then, we averaged the resulting binary segmentation maps for gray matter, white matter, and cerebral spinal fluid to create tissue probability maps. Finally, the tissue probability maps, which represent the probability that a voxel belongs to a class, were smoothed with a 1mm FWHM Gaussian smoothing kernel to form the prior probability maps (Figure 3; Evans et al., 1993; Evans et al., 1994).

### *Atlas Validation*

Our atlases were validated by comparing landmark location and distance measures (Black et al., 2001a; Black et al., 2001b). First, each monkey was normalized to the 112RM-SL atlas. Next, the middle of the anterior commissure, the middle of the posterior commissure, the anterior extent of the left and right caudate, and the lateral and medial inflection points on the central sulcus were identified in each monkey (Figure S2). Table 2 reports the mean landmarks for the D99-SL atlas and the 112RM-SL atlas. Next, we computed the distance of each monkey’s landmark to that of the 112RM-SL atlases (Table 3).

To address the question about possible artifacts or bias arising from a multi-center with different scanner strengths, anesthesia protocols, receiver coils, image resolutions, or pulse sequences; we investigated the image properties after normalization. The first step was to qualitatively investigate the histograms of each cohort to identify any potentially shifts in the data. Next, we statistically compared the number of voxels for each tissue type and their mean intensities

using pair-wise T-tests within six spherical regions with an 8mm radius to look at the images on a regional basis. The regions were centered at (-11, 30.5, 21), (10.5, 30.5, 21), (-16, 44.5, 2.5), (15.5, 44.5, 2.5), (-11.5, 76, 21.5), and (10.5, 76, 21.5). To identify differences on either in the global or region comparison, we used a liberal threshold of  $p < 0.05$  corrected for 3 tests since we were not concerned about type 1 errors.

### *Applications – Segmentation*

We segmented all the individual rhesus macaques from the UW cohort using several standardized segmentation algorithms that produce images of the probability of a voxel belonging to a given tissue class (e.g. gray matter) to demonstrate the application of the atlas and priors in segmentation (Figure 4). First, we used the “segment” tool in SPM5 to perform a unified segmentation using the prior probability maps (Ashburner and Friston, 2000, 2005). Next, we performed the segmentation without our prior probability maps using the “fast” tool in FSL (Zhang et al., 2001, also <http://fmrib.ox.ac.uk/analysis/techreport/#TR01YZ1>). The gray matter segments were used to estimate the transformation matrix to the 112RM-SL atlas space using the gray matter prior as a reference. The FSL segmentation maps were then normalized using the transformation matrix and subsequently modulated (to correct for local expansion or contraction) by multiplying voxel values in the segmented images by the Jacobian determinants derived from the spatial normalization (Good et al., 2001).

### *Applications – Multimodal Imaging*

We show that normalizing a T1-weighted scan to the T1-weighted 112RM-SL atlas and a T2-weighted scan from the same monkey to the T2-weighted atlas results in good alignment between modalities (Figure 5).

### *Applications – Cortical Surfaces*

While the goal of this project is to develop a population-averaged volume atlas, we have also recognized the growing importance of surface-based analyses. Van Essen and colleagues have already created surface-based atlases for several primate species (Van Essen, 2002, 2005; Van Essen et al., 2001b; Vincent et al., 2007). Their rhesus macaque surface (F99) is not aligned to either the D99-SL or 112RM-SL atlas. To facilitate integration of the surface- and volume-based atlases, we created a 12-parameter affine transformation to match our atlas to the F99 space. Notably, this integration will allow interspecies comparison by using surface-registration approaches which align different shaped cortices more accurately (Van Essen, 2005; Van Essen and Dierker, 2007).

## **Results**

### *Atlases*

Using the processing stream outlined in Figure 1, we formed a T1-weighted atlas, 112RM-SL, (Figure 2 middle,

<http://sumsdb.wustl.edu/sums/directory.do?id=X> and

<http://www.brainmap.wisc.edu/monkey.html>), which is in register with the single-subject D99-SL atlas (Figure 2 top) and thus are explicitly associated with published histology (Saleem and Logothetis, 2006). Figure 2 (bottom) illustrates the T2-weighted atlas, which is also in register with the single subject D99-SL atlas.

### *Prior Probability Maps*

We formed probabilistic tissue classification maps from the OHSU and UW cohorts (Figure 3B). These prior probability maps are the average of the binary segmentations (e.g. Figure 3A) of the individuals' contributing to each atlas.

### *Validation and Cohort Effects*

The landmarks in the 112RM-SL atlas are almost identical to those in the D99-SL atlas (Table 2). The high correspondence allows the use of the published histology accompanying the D99-SL atlas (Saleem and Logothetis, 2006). Additionally, we tested the monkey-to-atlas process for each of the monkeys used to create the atlas (Table 3). Variability, defined as the absolute value between the atlas landmark and the same landmark in an individual monkey, was consistent with previously published data (Black et al., 2001a; Black et al., 2001b). The mean intra-class correlation coefficient (ICC) within-rater was .96 (Fleiss, 1999). Between raters, the mean ICC was .93; thus the landmarks were reliably detected and consistent between observers.

Figure S1 shows the whole brain histograms for all voxels and separated by tissue type. Notably, the OHSU and UW cohorts showed very similar histograms, while the NIA cohort's histogram was shifted to the right for the gray matter and cerebral spinal fluid. These histograms led to quantifying the image properties in six spherical regions of interest. In summary, the NIA cohort had more voxels classified as white matter and the mean intensities in the gray matter were consistently higher than either the OHSU or UW cohorts (Supplement 1). Additionally, there were no significant differences ( $p > .0167$ ) in the number of voxels classified as CSF between any of the cohorts; however, the mean signal in the CSF from the NIA was substantially higher. While there were some differences between the OHSU and UW cohorts, they were minor compared to the aforementioned differences. Both the OHSU and UW data were acquired with volume coils at 3.0 T, compared to a surface-coil at 1.5 T for the NIA cohort. We conclude that scanner strength and/or receiver coil has the largest impact on the image properties. As a result, the poor contrast and potential misclassification tissue from animals in the NIA cohort, we chose to exclude them from the tissue probability maps. However, their inclusion in the general atlas increases its generalizability across scanner strengths and receiver coils. Their inclusion is also supported by the fact that the amount of brain tissue (gray plus white) was similar across all cohorts.

### *Applications - Segmentation*

We successfully segmented all the individual rhesus macaques from the validation group using the “segment” tool in SPM5 (Ashburner and Friston, 2000, 2005; Vincent et al., 2007) and the “fast” tool in FSL with and without the use of the prior probability maps (Zhang et al., 2001, also <http://fmrib.ox.ac.uk/analysis/techreport/#TR01YZ1>). The results of using the “segment” tool in SPM5 and the “fast” tool from a single individual are illustrated in Figure 4. SPM5 produces modulated images with voxel values representing the volume of tissue as a percentage of voxel volume in addition to unmodulated images that represent the posterior probability of each tissue type at that voxel. Qualitative comparisons of the values in the modulated images revealed subtle differences that are likely attributable to the when the spatial normalization is done (unified versus after segmentation for SPM and FSL, respectively), the use of priors, and segmentation algorithms (mixture of Gaussians versus mixture of Gaussian plus neighboring voxel and hidden markov random fields for SPM and FSL, respectively). The optimal segmentation and normalization methods and parameters for NHP should be investigated further, but are outside of the scope of this paper.

Recently, Alexander and colleagues completed a voxel-based morphometric (VBM) study of age in nineteen rhesus macaques (Alexander et al., 2008) using SPM5 with priors generated from their animals. Importantly, that study demonstrated that VBM can be applied to studies of aging in NHP to provide evidence of structural changes with age. However, an accessible standard rhesus macaque atlas space did not exist when they reported their

results, precluding the reporting of findings in coordinate space, and potentially affecting the generalizability of their findings.

#### *Applications – Multimodal registration*

We demonstrate excellent registration of T1- and T2- weighted images in Figure 5 and Figure S3. The normalized images and atlases are provided at <http://brainmap.wisc.edu/monkey.html>.

#### *Applications -- Cortical Surfaces*

Van Essen and colleagues previously created a cortical surface from a single rhesus macaque (Van Essen, 2002; Van Essen and Dierker, 2007; Van Essen et al., 2001a). Instead of creating another surface atlas, we created transformation matrices to convert the surface atlas space to the 112RM-SL atlas space and vice versa ([http://brainmap.wisc.edu/112RM-SL\\_to\\_F99\\_sn.mat](http://brainmap.wisc.edu/112RM-SL_to_F99_sn.mat) and [http://brainmap.wisc.edu/F99\\_to\\_112RM-SL\\_sn.mat](http://brainmap.wisc.edu/F99_to_112RM-SL_sn.mat)). The transformations are described below:

##### **112RM-SL to F99:**

$$\begin{aligned} X1 &= 1.029 * X + 0.009 * Y - 0.023 * Z + 0.754 \\ Y1 &= -0.031 * X + 1.046 * Y - 0.129 * Z - 21.177 \\ Z1 &= 0.012 * X + 0.167 * Y + 1.007 * Z - 15.422 \end{aligned}$$

##### **F99 to 112RM-SL:**

$$\begin{aligned} X1 &= 0.970 * X - 0.011 * Y + 0.021 * Z - 0.650 \\ Y1 &= 0.027 * X + 0.935 * Y + 0.120 * Z + 21.651 \\ Z1 &= -0.016 * X - 0.155 * Y + 0.971 * Z + 11.734 \end{aligned}$$

These transformations allow the integration of the population-average volume atlases with the existing surface atlas.

## **Discussion**

### *Species-Specific Atlases*

The dramatic variation in global brain volume within the *Macaca* genus (fascicularis [left hemisphere - 29.37 cc] < mulatta [80 cc] < nemestrina [97.7 cc]) suggests the need to have separate atlases for different species (Dorph-Petersen et al., 2005; Franklin et al., 2000; Malkova et al., 2006). Martin and Bowden suggest that the size differences may be correctable by global scaling; however, they acknowledge that their analysis was limited to the brainstem region and not the entire cortex (Bowden, 2000). More recently, reports have been published documenting variations in endocranial volume (Kirk, 2006) and sulcal patterns (Van Der Gucht et al., 2006) that necessitate species-specific atlases as these cannot be corrected for using affine-transformations.

Additionally, there are differences in the shape of the inferior frontal cortex between fascicularis and rhesus macaques (Figure S4). With the addition of this atlas collection, there are now three *Macaca* species that have population-average MRI-based atlases: N2K atlas for *Macaca nemestrina* (Black et al., 2001a, 2004), F6 atlas for *Macaca fascicularis* (Vincent et al., 2007), and the SL atlas collection, reported here, for *Macaca mulatta*. Most importantly, the population-average MRI-based SL atlases provide a standardized coordinate space to report *Macaca mulatta* species imaging findings in addition to an accompanying T2-weighted and surface-based templates.

### *Atlas Attributes*

It has been proposed that a brain atlas should optimize nine attributes: It should have high spatial resolution, identify cortical areas, be probabilistic, provide a standard coordinate space, link to existing atlases, be readily accessible, easily visualized (both volumes and surfaces), be extensible, and link to a database for experimental data (Frackowiak et al., 1997; Van Essen and Dierker, 2007).

The D99-SL atlas is a combined histology and high-resolution MRI atlas of the rhesus macaque (Saleem and Logothetis, 2006). Each 0.5 mm MRI slice has an accompanying set of histological sections and drawing of the cytoarchitecture. By using D99-SL atlas, we can link existing knowledge of histology or cortical areas to the probabilistic atlases. While the histology is from a single monkey, future studies may be able to utilize the population-average atlases to create probabilistic maps of the cytoarchitecture in rhesus macaques similar to what has been created in humans in recent years (Amunts et al., 2007; Caspers et al., 2006; Eickhoff et al., 2006a; Eickhoff et al., 2006b; Fischl et al., 2007).

The atlases described here maintain the stereotaxic coordinate space of D99-SL leading to several benefits. First, by maintaining a common standardized space, researchers from different laboratories and/or institutions can report their findings in the same coordinate system, analogous to the use of a standardized space such as MNI (Mazziotta et al., 2001; Mazziotta et al., 1995) for human studies. Secondly, the creation of a population-average atlas does not bias the

registration procedure towards the shape of any one monkey resulting in a better alignment across many individuals (Woods et al., 1999; Woods et al., 1998a; Woods et al., 1998b). These atlases can be used to align many individual monkeys together to carry out voxel-based analyses (Ashburner et al., 1998; Friston et al., 1999a; Friston et al., 1999b; Woods, 1996; Zeffiro et al., 1997) and such analyses could potentially be conducted with existing tools such as FSL and SPM (Alexander et al., 2008; Ashburner, 2007; Ashburner and Friston, 2000; Good et al., 2001).

These atlases and group-wise probability maps are publicly available through several sources including SumsDB (<http://sumsdb.wustl.edu/sums/directory.do?id=X>), the University of Wisconsin (<http://brainmap.wisc.edu/monkey.html>) the SPM website (<http://www.fil.ion.ucl.ac.uk/spm/ext/>). The images are stored in NIFTI format (<http://nifti.nih.gov/nifti-1/>) to preserve the stereotaxic origin and space and can be viewed in many standard imaging software packages that support NIFTI (e.g. SPM (University College London, London, UK), FSL (Analysis Group, FMRIB, Oxford, UK; see -- Smith et al., 2004), CARET (Washington University, St. Louis, MO; see -- Van Essen et al., 2001a), and ANALYZE 8.1 (Mayo Clinic, Rochester, MN; see -- Robb, 2001)). Future studies should develop population-averaged cortical surfaces of these atlas volumes to allow researchers the ability to conduct studies of the cortical surface in non-human primates (Van Essen, 2005). Additionally, methods already established by Van Essen and colleagues would allow population-average, landmark-based surfaces of the rhesus

macaque to be used to compare them to humans via cortical surface mapping (Van Essen and Dierker, 2007; Van Essen et al., 2001a; Van Essen et al., 2001b).

The methods described here could be adapted to allow the current atlases to be expanded or create new atlases that would encompass a larger or narrower age range (e.g. juveniles), yet be directly comparable to the existing atlases and the D99-SL histology (Saleem and Logothetis, 2006). In humans, it has been suggested that age-specific atlases should be developed and used in the analysis of age-related changes (Van Essen and Dierker, 2007; Wilke et al., 2008). While we feel that the Template-O-Matic (<http://dbm.neuro.uni-jena.de/software/tom/>) is an excellent tool for creating age-specific atlas; only 112 monkeys contributed to this atlas, compared to over 400 children that contributed the development of the software package, which may limit its utility. Alternatively, researchers can use the priors and the DARTEL toolbox in SPM to create study-specific atlases that would still be aligned to the 112RM-SL atlas space (Ashburner, 2007).

We also created a T2-weighted atlas and demonstrated its ability to be used to normalize T2-weighted scans; however, it would be more advantageous to have atlases for additional modalities (e.g. diffusion-weighted and positron emission tomography), and this will also be the focus of future work. The inclusion of multi-modal atlases increases the utility of that the D99-SL stereotaxic space for reporting results, thereby enabling a more comprehensive and integrated view of the macaque brain anatomy and function (Toga et al.,

2006). Finally, electrophysiological data could be mapped to the probabilistic atlases using MR-guided electrophysiology or identifying the electrode positions on an MRI after the experiment has been completed (Frey et al., 2004; Kalwani et al., 2008; Scherberger et al., 2003; Sultan et al., 2007; Tolias et al., 2005); thus adding to our understanding of different brain regions.

We envision that experimental data collected and aligned to these atlases will be made available through SumsDB and/or another image databases encouraging meta-analyses of rhesus macaque studies. Furthermore, there is more than 35 years of electrophysiology and histology work that is unparalleled in humans that can be potentially incorporated into these atlases (Crick and Jones, 1993; Kalwani et al., 2008).

#### *Limitations and Concerns*

These atlases are only applicable to studies of the rhesus macaque (*Macaca mulatta*); atlases for a handful of other species already exist as described above. Additionally, our atlases only contain adult monkeys and may not be generalizable to juvenile rhesus macaques. Although the ratio of males to females in this atlas is not optimal, it is approximately equal to that used in human atlases (Evans et al., 1993; Evans et al., 1994; Mazziotta et al., 2001; Mazziotta et al., 1995). The largest cohort effects found in the present study were between the cohorts scanned at high field versus the cohort scanned at low field. The effect likely represents a difference due to scanner strength (3.0T versus 1.5T) or receiver coil. While this is a clear limitation, we included all available subjects in the atlas space to enhance its generalizability across different data

acquisition scenarios. Our prior gray and white matter maps used only the 3.0T scans for more valid tissue segmentation.

### *Conclusion*

Brain imaging in non-human primates is becoming increasingly common for many experimental applications. Here we present a brain atlas collection for the adult rhesus macaque (*Macaca mulatta*) and review methods for creating multi-modal atlases using an infrastructure that will allow voxel- and surface-based approaches that are common in human brain mapping studies to be readily applied to non-human primate studies. More importantly, these atlases provide a standardized space that will allow researchers from different institutions to report coordinate results in a standard space and directly compare their results.

### **Acknowledgements**

This study was supported in part by the National Institutes of Health RR000167 (UW), AG11915(UW), AG000213 (UW), GM007507(UW), RR00163 (ONPRC), AG029612 (OHSU) and the Intramural Research Program of the National Institute on Aging. This study was also supported with resources and use of facilities at the William S. Middleton Memorial Veterans Hospital, Madison, WI, USA. John Matochik is now at the National Institute on Alcohol Abuse and Alcoholism. The assistance of Erik K. Kastman, Brent W. Thiel, Michele E. Fitzgerald, Ron Fisher, Scott T. Baum, Josh Smith, Ricki J Colman, Ph.D., Andy. A. Alexander, Ph.D., Barbara B. Bendlin, Ph.D. and the Waisman Center for

Brain Imaging was greatly appreciated. We would especially like to thank Drs. Kadharbatcha S. Saleem and Nikos K. Logothetis for providing a digital copy of the D99-SL atlas.

## Figure Legends

Figure 1: Atlas Creation Pipeline. Image processing stream for non-human primate probabilistic atlases. The iterative procedure utilizes four registration steps to improve alignment between the individuals contributing to the atlas. (1) In the first registration step, the target volume is the D99-SL atlas; (2) the average of the registered individuals is registered to the D99-SL atlas; (3) in the second iteration, the target volume is average template from step (2); (4) the individuals are then averaged a second time and that average is registered to the D99-SL atlas. This ensures that the probabilistic atlas is in register with the published D99-SL atlas.

Figure 2: Multi-modal Rhesus Macaque Atlases. Axial slices from  $Z=0$  mm to  $Z=40$  mm in 5 mm increments. Top: D99-SL atlas; middle: 112RM-SL T1-weighted atlas; and bottom: T2-weighted atlas.

Figure 3: Tissue Probability Maps. Axial slices from  $Z=2.5$  mm to  $Z=32.5$  mm in 10 mm increments showing the tissue probabilities for gray matter, white matter, and cerebral spinal fluid (CSF). These prior probability maps were formed from averaging binary coded segmentation images from the OHSU and UW animals and smoothing the averages with a 1 mm FWHM Gaussian filter.

Figure 4: Segmentation of an Individual Rhesus Macaque. Top: A horizontal slice of an individual rhesus macaque T1-weighted MRI scan in atlas space at Z=20mm. Bottom Sets: gray and white matter probability maps for three different segmentation methods. Note that FSL provides a crisper separation between tissue classes due to the inclusion of nearest neighbors in the algorithm, but not necessarily better. Additionally, note that the registration of the SPM and FSL maps are different due normalization methods (non-linear unified integrated with segmentation versus non-linear after segmentation using SPM and FSL, respectively). The scale bar is applicable to the SPM unmodulated as the probability of a voxel belonging to a specific tissue class with the maximum being 100%. The SPM modulated and FSL images are on the same scale, but should be interpreted as the volume of tissue at a given voxel as a percentage of the probability of the voxel belonging to a tissue, which can exceed 100.

Figure 5: Multimodal Application. Orthogonal slices through the origin. From top to bottom: 112RM-SL T1-weighted atlas; T1-weighted scan; T2-weighted scan; T2-weighted atlas. Note how the structures line up between modalities and the atlas. Images can be downloaded from: <http://brainmap.wisc.edu/monkey.html>.

Figure S1: Cohort intensity histograms (25 bins, each 12 units wide). The solid lines represent the mean of each cohort with the shaded region being 1 standard deviation above or below the mean. For each of the four graphs, an intensity histogram was created for each subject. These histograms were then used to

compute the cohort mean and standard deviation in each bin were calculated. We noted that the peak locations and heights were similar between the OHSU and UW cohorts, while the NIA cohort differed with respect to the grey matter (higher intensity) peak. Additionally, the highest intensity peak was similar across cohorts.

Figure S2: Central Sulcus Landmarks A: Orthogonal slices marking the left lateral central sulcus landmark (-24.5, 16, 20) from the D99-SL atlas. The crosshairs indicate the landmark in each of the three planes. This landmark is identified by finding the most anterior coronal slice that has the central sulcus reaching the surface in two locations. B: Orthogonal slices marking the left lateral central sulcus landmark (-16.5, 15.5, 26) from the D99-SL atlas. The crosshairs indicate the landmark in each of the three planes. This landmark is identified finding the coronal slice with the most medial aspect of the central sulcus that still has a sharp hook in it and placing the landmark at the inflection point. Note that both landmarks are at the depth of the sulcus in all three planes.

Figure S3: T1-weighted image with T2-weighted image overlaid. Axial slices from  $Z=-3$  to  $Z=37$  in 5mm increments are shown. T1-weighted underlay is displayed in grayscale. The T2-weighted overlay is in color with darker colors representing brain and the brighter intensity cerebral spinal fluid (CSF) shows up as green and orange. Note that the CSF from the T2-weighted image lines up with the sulci

and ventricles of the the T1-weighted image indicating that the T1- and T2-weighted images are in register with each other.

Figure S4: Cynomolgous macaque (*Macaca fascicularis*) atlas

(<http://www.nil.wustl.edu/labs/kevin/ni/cyno/>) normalized to the 112RM-SL rhesus macaque (*Macacca mulatta*) atlas (<http://brainmap.wisc.edu/monkey.html>) using a 12 parameter affine transformation. Sagittal slices from 0mm to 25mm in 5mm increments are shown. A red 10mmX10mm grid is overlaid to illustrate the structural differences. Notably, most of the differences occur in the frontal lobes. Light blue arrows highlight several of the differences including: anterior corpus callosum and the shape of the frontal pole. The shape differences indicate that linear registration is insufficient for comparing fascicularis and rhesus macaques.

## References

- Alexander, G.E., Chen, K., Aschenbrenner, M., Merkley, T.L., Santerre-Lemmon, L.E., Shamy, J.L., Skaggs, W.E., Buonocore, M.H., Rapp, P.R., Barnes, C.A., 2008. Age-related regional network of magnetic resonance imaging gray matter in the rhesus macaque. *J Neurosci* 28, 2710-2718.
- Amunts, K., Schleicher, A., Zilles, K., 2007. Cytoarchitecture of the cerebral cortex--more than localization. *Neuroimage* 37, 1061-1065; discussion 1066-1068.
- Ashburner, J., 2007. A fast diffeomorphic image registration algorithm. *Neuroimage* 38, 95-113.
- Ashburner, J., Friston, K.J., 2000. Voxel-based morphometry--the methods. *Neuroimage* 11, 805-821.
- Ashburner, J., Friston, K.J., 2005. Unified segmentation. *Neuroimage* 26, 839-851.
- Ashburner, J., Hutton, C., Frackowiak, R., Johnsrude, I., Price, C., Friston, K., 1998. Identifying global anatomical differences: deformation-based morphometry. *Hum Brain Mapp* 6, 348-357.
- Black, K.J., Gado, M.H., Videen, T.O., Perlmutter, J.S., 1997. Baboon basal ganglia stereotaxy using internal MRI landmarks: validation and application to PET imaging. *J Comput Assist Tomogr* 21, 881-886.
- Black, K.J., Koller, J.M., Snyder, A.Z., Perlmutter, J.S., 2001a. Template images for nonhuman primate neuroimaging: 2. Macaque. *Neuroimage* 14, 744-748.
- Black, K.J., Koller, J.M., Snyder, A.Z., Perlmutter, J.S., 2004. Atlas template images for nonhuman primate neuroimaging: baboon and macaque. *Methods Enzymol* 385, 91-102.
- Black, K.J., Snyder, A.Z., Koller, J.M., Gado, M.H., Perlmutter, J.S., 2001b. Template images for nonhuman primate neuroimaging: 1. Baboon. *Neuroimage* 14, 736-743.
- Bowden, D., Dubach, MF, 2000. Applicability of the Template Atlas to various primate species. In: Martin, R., Bowden, DM (Ed.), *Primate Brain Maps: Structure of the Macaque Brain*. Elsevier, New York.
- Busse, R.F., Hariharan, H., Vu, A., Brittain, J.H., 2006. Fast spin echo sequences with very long echo trains: design of variable refocusing flip angle schedules and generation of clinical T2 contrast. *Magn Reson Med* 55, 1030-1037.
- Cannestra, A.F., Santori, E.M., Holmes, C.J., Toga, A.W., 1997. A three-dimensional multimodality brain map of the nemestrina monkey. *Brain Res Bull* 43, 141-148.
- Caspers, S., Geyer, S., Schleicher, A., Mohlberg, H., Amunts, K., Zilles, K., 2006. The human inferior parietal cortex: cytoarchitectonic parcellation and interindividual variability. *Neuroimage* 33, 430-448.
- Crick, F., Jones, E., 1993. Backwardness of human neuroanatomy. *Nature* 361, 109-110.
- Davis, R., Huffman, R., 1968. *A Stereotaxic Atlas of the Brain of the Baboon*. Univ. Texas Press, Austin, TX.
- Devlin, J.T., Poldrack, R.A., 2007. In praise of tedious anatomy. *Neuroimage* 37, 1033-1041; discussion 1050-1038.

- Dorph-Petersen, K.A., Pierri, J.N., Perel, J.M., Sun, Z., Sampson, A.R., Lewis, D.A., 2005. The influence of chronic exposure to antipsychotic medications on brain size before and after tissue fixation: a comparison of haloperidol and olanzapine in macaque monkeys. *Neuropsychopharmacology* 30, 1649-1661.
- Eickhoff, S.B., Amunts, K., Mohlberg, H., Zilles, K., 2006a. The human parietal operculum. II. Stereotaxic maps and correlation with functional imaging results. *Cereb Cortex* 16, 268-279.
- Eickhoff, S.B., Schleicher, A., Zilles, K., Amunts, K., 2006b. The human parietal operculum. I. Cytoarchitectonic mapping of subdivisions. *Cereb Cortex* 16, 254-267.
- Evans, A.C., Collins, D.L., Mills, S.R., Brown, E.D., Kelly, R.L., Peters, T.M., 1993. 3D statistical neuroanatomical models from 305 MRI volumes. *IEEE--Nuclear Science Symposium and Medical Imaging Conference*, pp. 1813-1817.
- Evans, A.C., Kamber, M., Collins, D.L., MacDonald, D., 1994. An MRI-based probabilistic atlas of neuroanatomy. In: Shorvon, S., Fish, D., Anderman, F., Bydder, G.M., Stefan, H. (Eds.), *Magnetic Resonance Scanning and Epilepsy*. Plenum, New York, pp. 263-274.
- Fischl, B., Rajendran, N., Busa, E., Augustinack, J., Hinds, O., Yeo, B.T., Mohlberg, H., Amunts, K., Zilles, K., 2007. Cortical Folding Patterns and Predicting Cytoarchitecture. *Cereb Cortex*.
- Fischl, B., Sereno, M.I., Tootell, R.B., Dale, A.M., 1999. High-resolution intersubject averaging and a coordinate system for the cortical surface. *Hum Brain Mapp* 8, 272-284.
- Fleiss, J., 1999. *The design and analysis of clinical experiments*. John Wiley & Sons, Inc, New York.
- Fox, P.T., Perlmuter, J.S., Raichle, M.E., 1985. A stereotactic method of anatomical localization for positron emission tomography. *J Comput Assist Tomogr* 9, 141-153.
- Frackowiak, R.S.J., Friston, K.J., Frith, C.D., Dolan, R.J., Mazziotta, J.C., 1997. *Human Brain Function*. Academic Press, San Diego, CA.
- Franklin, M.S., Kraemer, G.W., Shelton, S.E., Baker, E., Kalin, N.H., Uno, H., 2000. Gender differences in brain volume and size of corpus callosum and amygdala of rhesus monkey measured from MRI images. *Brain Res* 852, 263-267.
- Frey, S., Comeau, R., Hynes, B., Mackey, S., Petrides, M., 2004. Frameless stereotaxy in the nonhuman primate. *Neuroimage* 23, 1226-1234.
- Friston, K.J., Holmes, A.P., Price, C.J., Buchel, C., Worsley, K.J., 1999a. Multisubject fMRI studies and conjunction analyses. *Neuroimage* 10, 385-396.
- Friston, K.J., Holmes, A.P., Worsley, K.J., 1999b. How many subjects constitute a study? *Neuroimage* 10, 1-5.
- Gold, G.E., Busse, R.F., Beehler, C., Han, E., Brau, A.C., Beatty, P.J., Beaulieu, C.F., 2007. Isotropic MRI of the knee with 3D fast spin-echo extended echo-train acquisition (XETA): initial experience. *AJR Am J Roentgenol* 188, 1287-1293.
- Good, C.D., Johnsrude, I.S., Ashburner, J., Henson, R.N., Friston, K.J., Frackowiak, R.S., 2001. A voxel-based morphometric study of ageing in 465 normal adult human brains. *Neuroimage* 14, 21-36.
- Greer, P.J., Villemagne, V.L., Ruszkiewicz, J., Graves, A.K., Meltzer, C.C., Mathis, C.A., Price, J.C., 2002. MR atlas of the baboon brain for functional neuroimaging. *Brain Res Bull* 58, 429-438.

- Jenkinson, M., Smith, S., 2001. A global optimisation method for robust affine registration of brain images. *Med Image Anal* 5, 143-156.
- Kalwani, R.M., Bloy, L., Elliott, M.A., Gold, J.I., 2008. A method for localizing microelectrode trajectories in the macaque brain using MRI. *J Neurosci Methods*.
- Kamber, M., Collins, D.L., Shinghal, R., Francis, G.S., Evans, A.C., 1992. Model-based 3D segmentation of multiple sclerosis lesions in dual-echo MRI data. In: Robb, R.A. (Ed.), *Second Conference on Visualization in Biomedical Computing*. SPIE, pp. 590-600.
- Kirk, E.C., 2006. Visual influences on primate encephalization. *J Hum Evol* 51, 76-90.
- Malkova, L., Heuer, E., Saunders, R.C., 2006. Longitudinal magnetic resonance imaging study of rhesus monkey brain development. *Eur J Neurosci* 24, 3204-3212.
- Martin, R.F., Bowden, D.M., 1996. A stereotaxic template atlas of the macaque brain for digital imaging and quantitative neuroanatomy. *Neuroimage* 4, 119-150.
- Mazziotta, J., Toga, A., Evans, A., Fox, P., Lancaster, J., Zilles, K., Woods, R., Paus, T., Simpson, G., Pike, B., Holmes, C., Collins, L., Thompson, P., MacDonald, D., Iacoboni, M., Schormann, T., Amunts, K., Palomero-Gallagher, N., Geyer, S., Parsons, L., Narr, K., Kabani, N., Le Goualher, G., Boomsma, D., Cannon, T., Kawashima, R., Mazoyer, B., 2001. A probabilistic atlas and reference system for the human brain: International Consortium for Brain Mapping (ICBM). *Philos Trans R Soc Lond B Biol Sci* 356, 1293-1322.
- Mazziotta, J.C., Toga, A.W., Evans, A., Fox, P., Lancaster, J., 1995. A probabilistic atlas of the human brain: theory and rationale for its development. The International Consortium for Brain Mapping (ICBM). *Neuroimage* 2, 89-101.
- Mikula, S., Trotts, I., Stone, J.M., Jones, E.G., 2007. Internet-enabled high-resolution brain mapping and virtual microscopy. *Neuroimage* 35, 9-15.
- Paxinos, G.H., X.F., and Toga, A.W., 2000. *The Rhesus Monkey Brain in Stereotaxic Coordinates*. Academic Press, London.
- Robb, R.A., 2001. The biomedical imaging resource at Mayo Clinic. *IEEE Trans Med Imaging* 20, 854-867.
- Saleem, K.S., Logothetis, N.K., 2006. *A Combined MRI and Histology Atlas of the Rhesus Monkey Brain*. Academic Press, Amsterdam.
- Scherberger, H., Fineman, I., Musallam, S., Dubowitz, D.J., Bernheim, K.A., Pesaran, B., Corneil, B.D., Gilliken, B., Andersen, R.A., 2003. Magnetic resonance image-guided implantation of chronic recording electrodes in the macaque intraparietal sulcus. *J Neurosci Methods* 130, 1-8.
- Smith, S.M., Jenkinson, M., Woolrich, M.W., Beckmann, C.F., Behrens, T.E., Johansen-Berg, H., Bannister, P.R., De Luca, M., Drobnjak, I., Flitney, D.E., Niaz, R.K., Saunders, J., Vickers, J., Zhang, Y., De Stefano, N., Brady, J.M., Matthews, P.M., 2004. Advances in functional and structural MR image analysis and implementation as FSL. *Neuroimage* 23 Suppl 1, S208-219.
- Sultan, F., Augath, M., Logothetis, N., 2007. BOLD sensitivity to cortical activation induced by microstimulation: comparison to visual stimulation. *Magn Reson Imaging* 25, 754-759.
- Toga, A.W., Thompson, P.M., Mori, S., Amunts, K., Zilles, K., 2006. Towards multimodal atlases of the human brain. *Nat Rev Neurosci* 7, 952-966.

- Tolias, A.S., Sultan, F., Augath, M., Oeltermann, A., Tehovnik, E.J., Schiller, P.H., Logothetis, N.K., 2005. Mapping cortical activity elicited with electrical microstimulation using fMRI in the macaque. *Neuron* 48, 901-911.
- Van Der Gucht, E., Youakim, M., Arckens, L., Hof, P.R., Baizer, J.S., 2006. Variations in the structure of the prelunate gyrus in Old World monkeys. *Anat Rec A Discov Mol Cell Evol Biol* 288, 753-775.
- Van Essen, D.C., 2002. Surface-based atlases of cerebellar cortex in the human, macaque, and mouse. *Ann N Y Acad Sci* 978, 468-479.
- Van Essen, D.C., 2004. Surface-based approaches to spatial localization and registration in primate cerebral cortex. *Neuroimage* 23 Suppl 1, S97-107.
- Van Essen, D.C., 2005. A Population-Average, Landmark- and Surface-based (PALS) atlas of human cerebral cortex. *Neuroimage* 28, 635-662.
- Van Essen, D.C., Dierker, D.L., 2007. Surface-based and probabilistic atlases of primate cerebral cortex. *Neuron* 56, 209-225.
- Van Essen, D.C., Drury, H.A., Dickson, J., Harwell, J., Hanlon, D., Anderson, C.H., 2001a. An integrated software suite for surface-based analyses of cerebral cortex. *J Am Med Inform Assoc* 8, 443-459.
- Van Essen, D.C., Lewis, J.W., Drury, H.A., Hadjikhani, N., Tootell, R.B., Bakircioglu, M., Miller, M.I., 2001b. Mapping visual cortex in monkeys and humans using surface-based atlases. *Vision Res* 41, 1359-1378.
- Vincent, J.L., Patel, G.H., Fox, M.D., Snyder, A.Z., Baker, J.T., Van Essen, D.C., Zempel, J.M., Snyder, L.H., Corbetta, M., Raichle, M.E., 2007. Intrinsic functional architecture in the anaesthetized monkey brain. *Nature* 447, 83-86.
- Wilke, M., Holland, S.K., Altaye, M., Gaser, C., 2008. Template-O-Matic: a toolbox for creating customized pediatric templates. *Neuroimage* 41, 903-913.
- Woods, R.P., 1996. Modeling for intergroup comparisons of imaging data. *Neuroimage* 4, S84-94.
- Woods, R.P., Dapretto, M., Sicotte, N.L., Toga, A.W., Mazziotta, J.C., 1999. Creation and use of a Talairach-compatible atlas for accurate, automated, nonlinear intersubject registration, and analysis of functional imaging data. *Hum Brain Mapp* 8, 73-79.
- Woods, R.P., Grafton, S.T., Holmes, C.J., Cherry, S.R., Mazziotta, J.C., 1998a. Automated image registration: I. General methods and intrasubject, intramodality validation. *J Comput Assist Tomogr* 22, 139-152.
- Woods, R.P., Grafton, S.T., Watson, J.D., Sicotte, N.L., Mazziotta, J.C., 1998b. Automated image registration: II. Intersubject validation of linear and nonlinear models. *J Comput Assist Tomogr* 22, 153-165.
- Zeffiro, T.A., Eden, G.F., Woods, R.P., VanMeter, J.W., 1997. Intersubject analysis of fMRI data using spatial normalization. *Adv Exp Med Biol* 413, 235-240.
- Zhang, Y., Brady, M., Smith, S., 2001. Segmentation of brain MR images through a hidden Markov random field model and the expectation-maximization algorithm. *IEEE Trans Med Imaging* 20, 45-57.

Figure 1

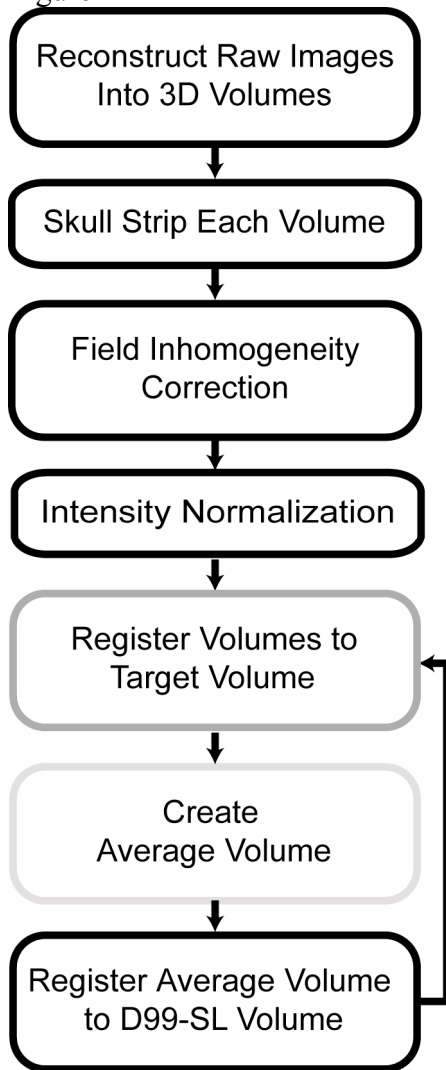


Figure 2

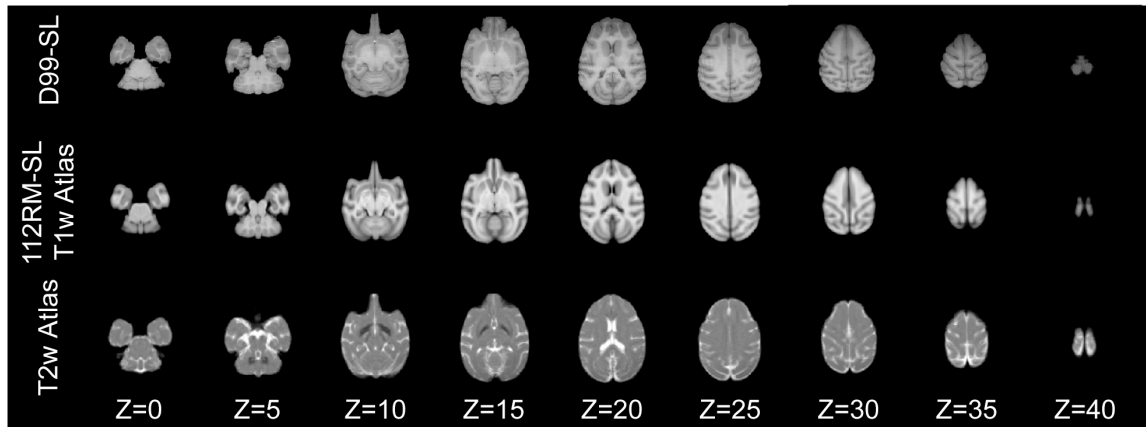


Figure 3

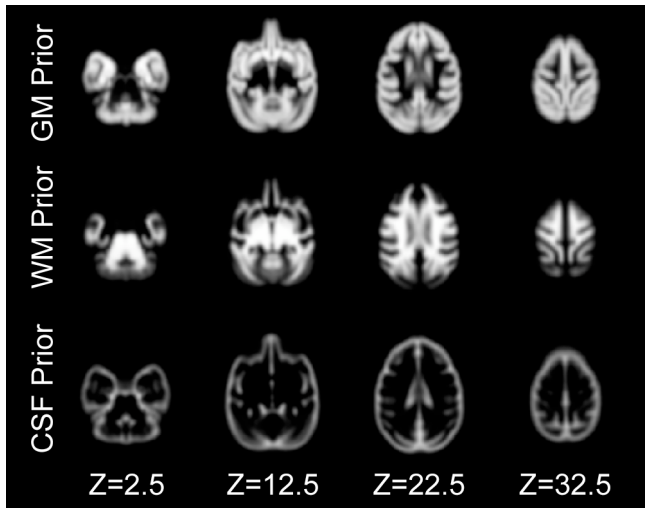


Figure 4

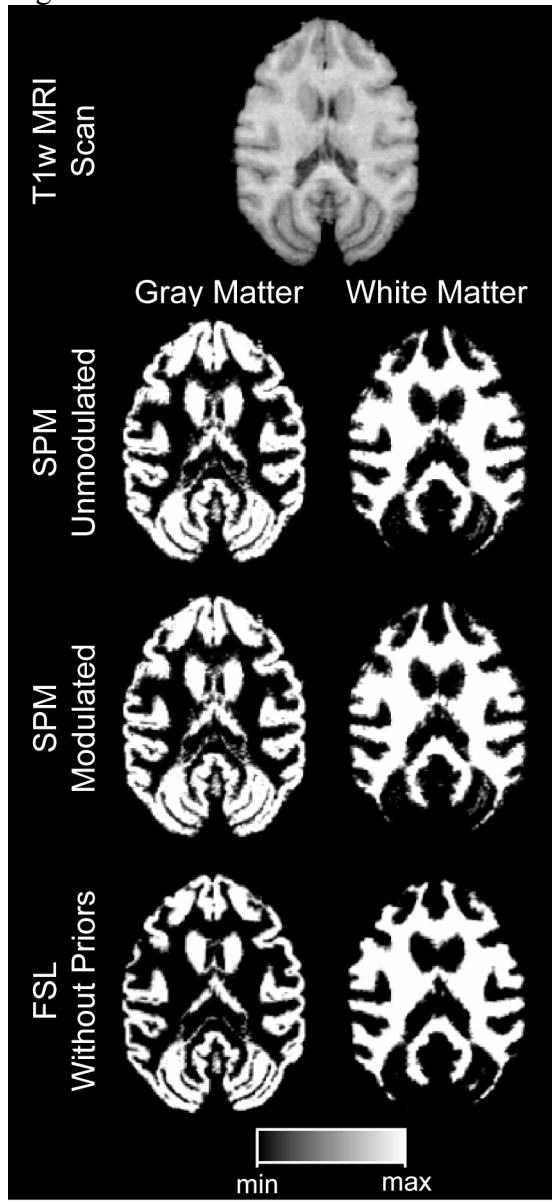


Figure 5

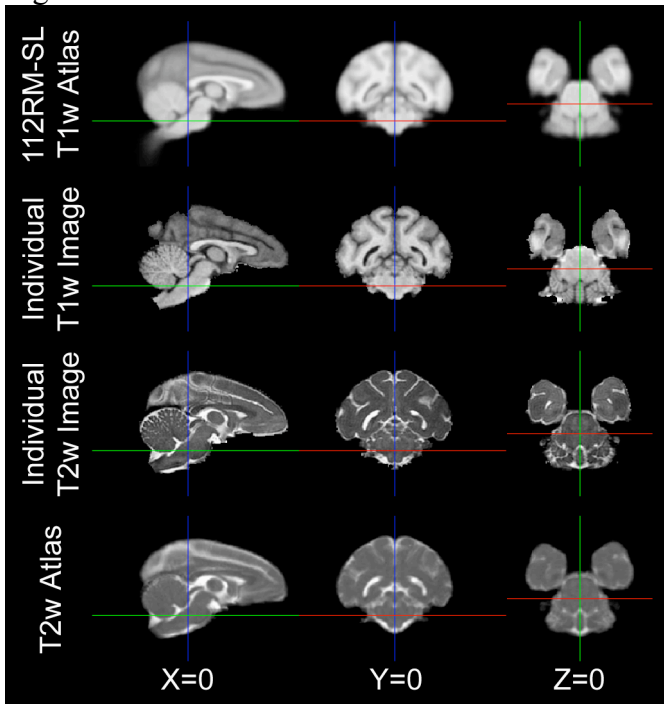


Figure S1

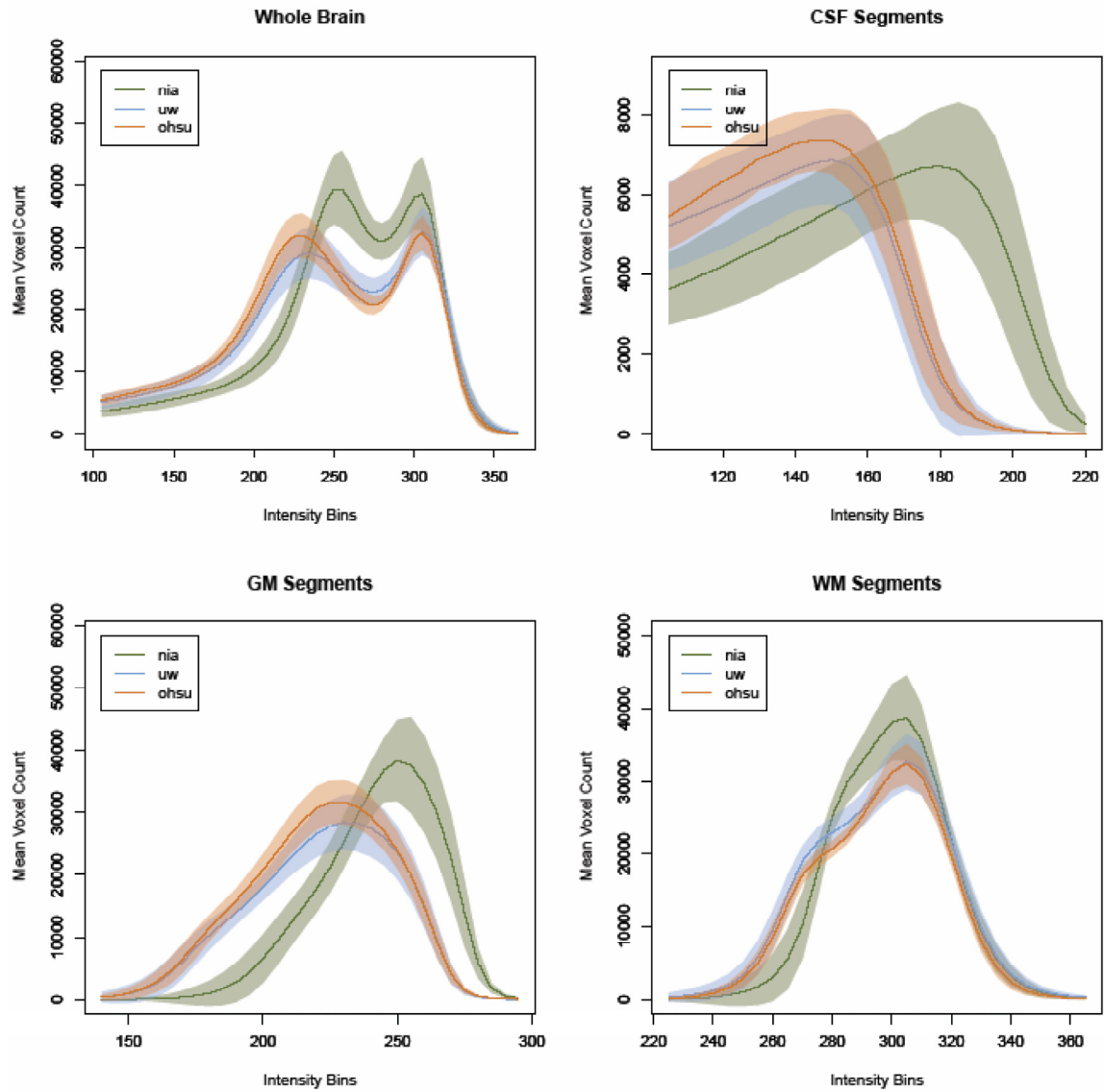


Figure S2

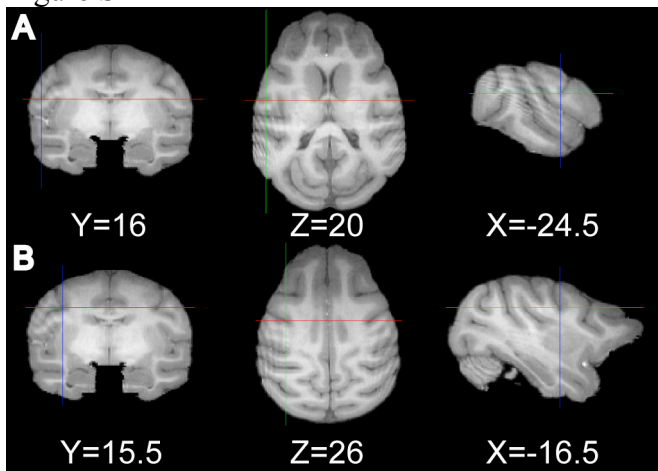


Figure S3

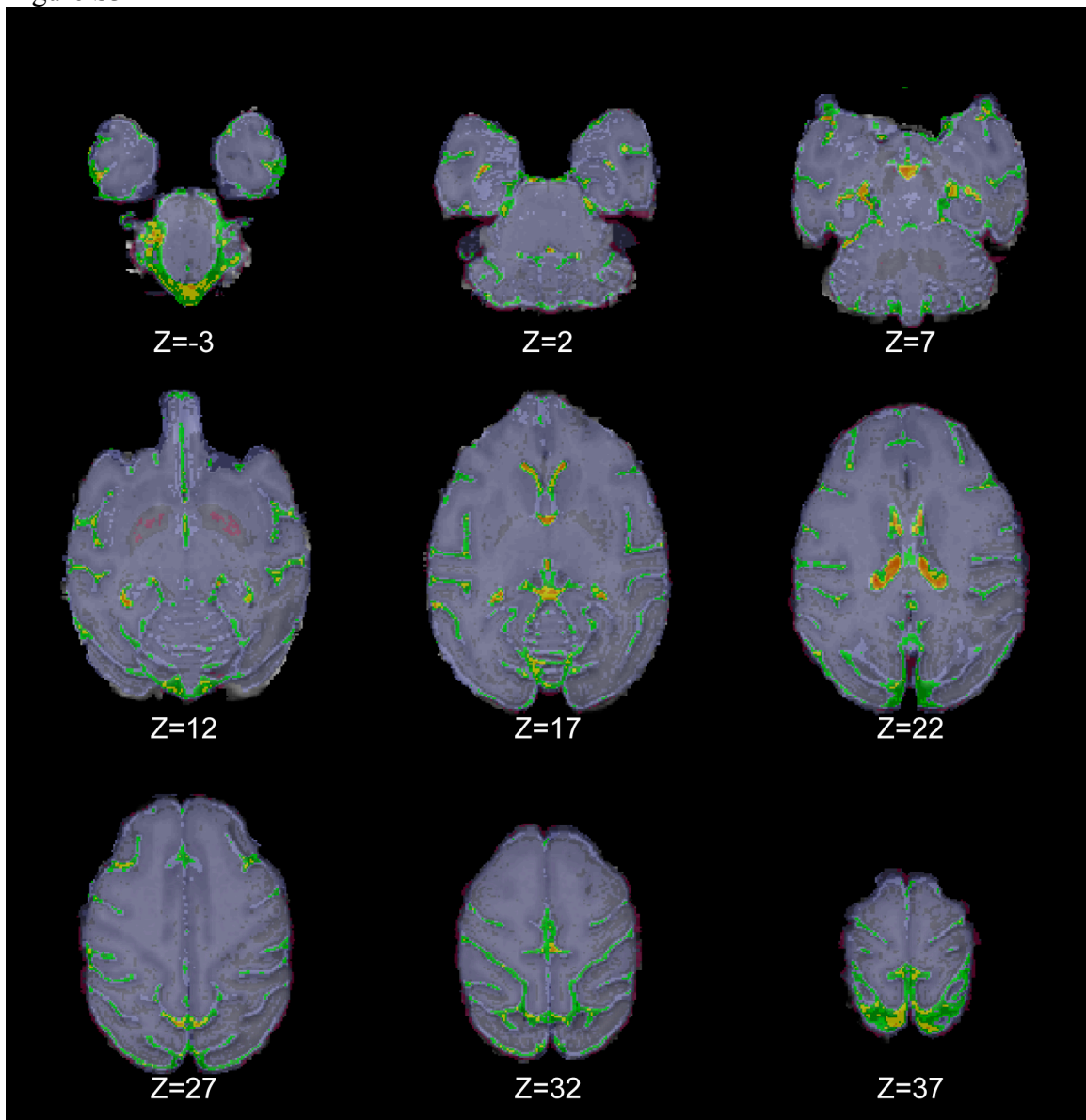


Figure S4

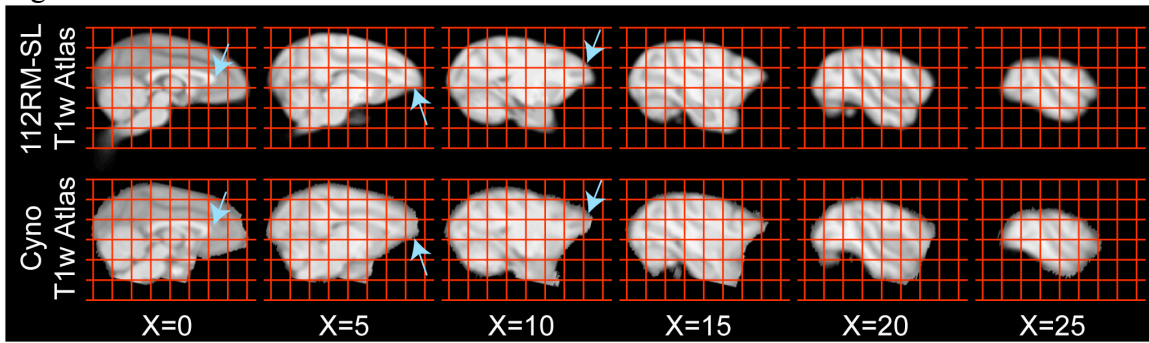


Table 1

---

Table 1. Rhesus macaque (*Macaca mulatta*) atlas demographics

Age in Months	NIA	Cohort	
		UW	OHSU
<i>N</i>	60	37	15
<i>Gender (m/f)</i>	60/0	19/18	3/12
Minimum	39	132	52
Mean	214	280	222
Maximum	432	346	344
SD	97	54	98

---

Table 2

<b>TABLE 2. Atlas Landmark Locations</b>						
<b>Landmark</b>	<b>112RM-SL T1-weighted Atlas</b>			<b>D99-SL Atlas</b>		
	x	y	z	x	y	z
AC	0.00	21.00	12.00	-0.50	20.00	13.00
PC	0.00	7.50	14.00	0.00	6.50	14.50
L. ant. Caudate	-6.50	33.00	17.50	-6.50	32.50	18.00
R. ant. Caudate	6.00	33.00	17.50	5.50	32.50	18.00
L. lat. Cs	-24.50	16.50	20.50	-24.00	16.50	20.50
R. lat. Cs	23.50	17.00	20.50	23.50	17.50	19.50
L. med. Cs	-18.00	15.00	25.50	-17.00	15.50	25.50
R. med. Cs	18.00	16.50	25.00	17.00	16.50	25.00

Notes: All values are in millimeters; AC, anterior commissure; PC, posterior commissure; ant. caudate, anterior extent of the caudate nucleus; lateral Cs, lateral inflection point of the central sulcus; medial Cs, medial inflection point of the central sulcus.

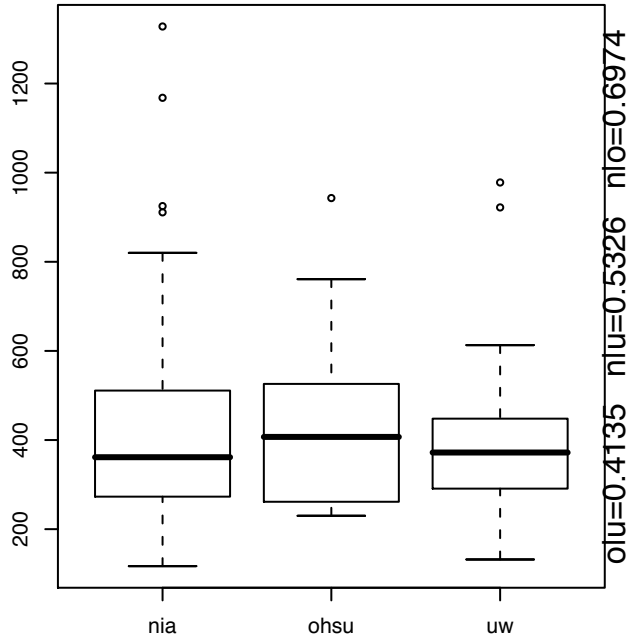
Table 3

<b>Table 3. Landmark Variation (Distance Between Atlas and Individuals)</b>		
Landmark	Mean	Max
AC	0.8	1.87
PC	0.8	2.24
L. ant. Caudate	1.12	2.29
R. ant. Caudate	1.13	2.96
L. ICs	1.74	6.1
R. ICs	1.83	5.68
L. mCs	1.78	6
R. mCs	2.07	6.2

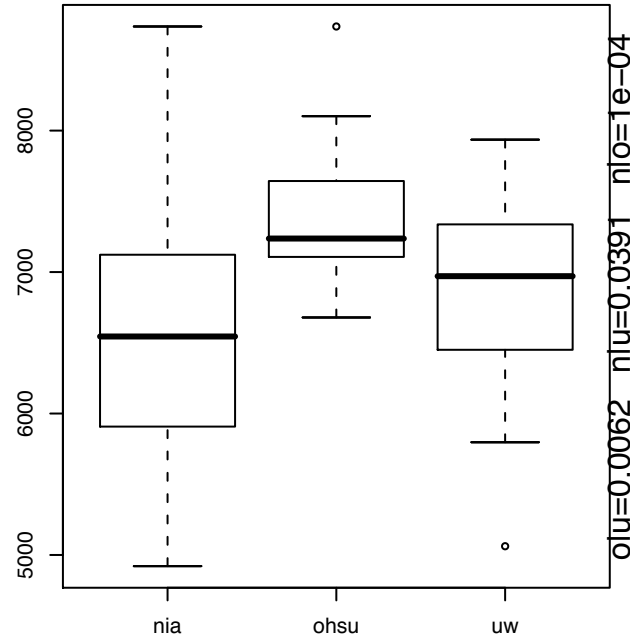
Notes: All values are in millimeters; AC, anterior commissure; PC, posterior commissure; ant. caudate, anterior extent of the caudate nucleus; ICs, lateral inflection point of the central sulcus; mCs, medial inflection point of the central sulcus.

Supplement

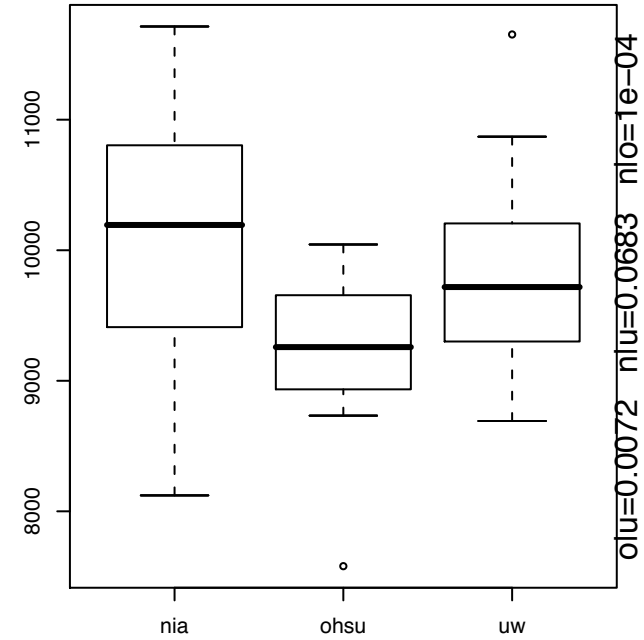
L.frontal csf voxels



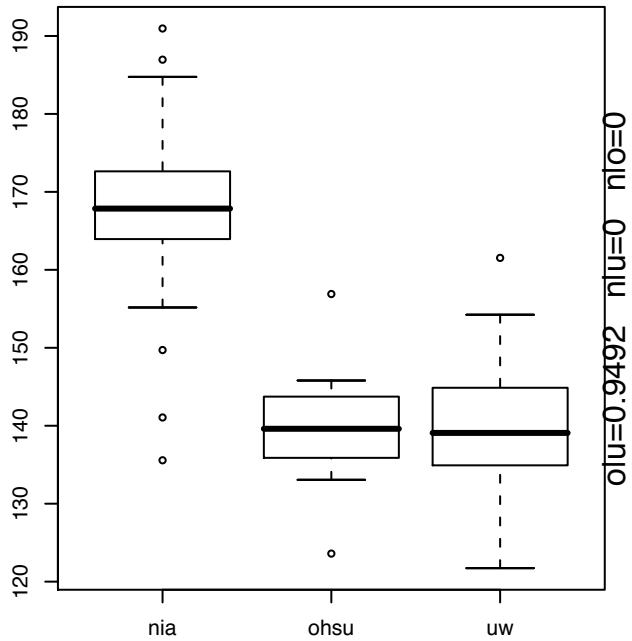
L.frontal gm voxels



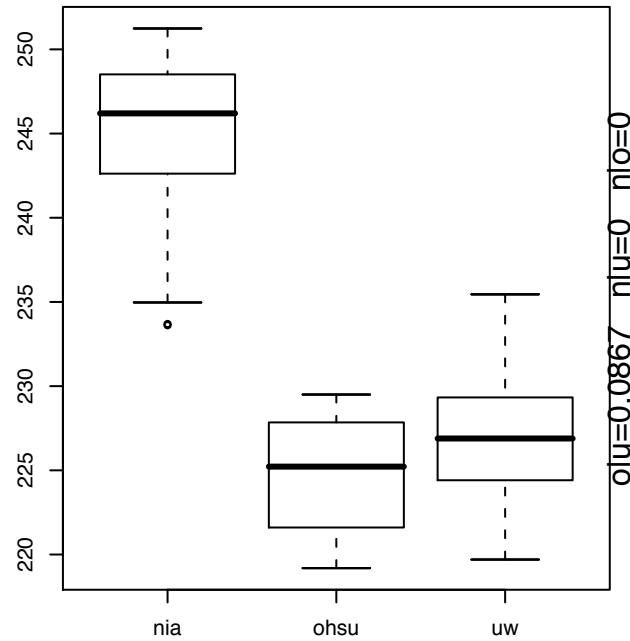
L.frontal wm voxels



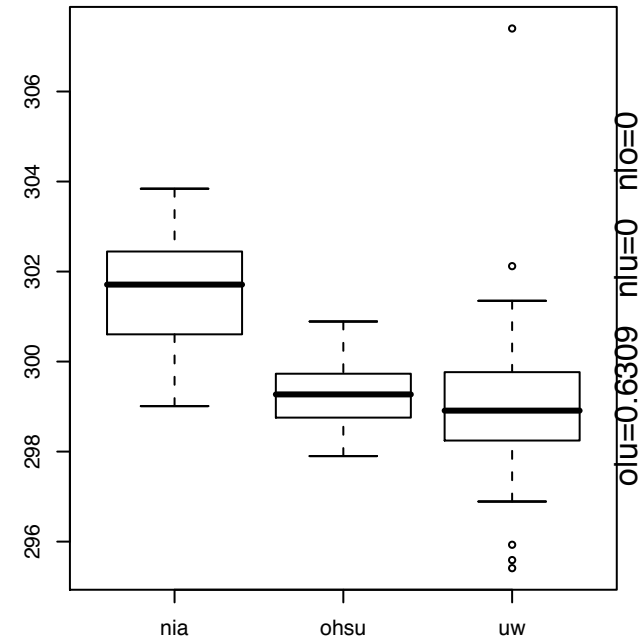
L.frontal csf mean



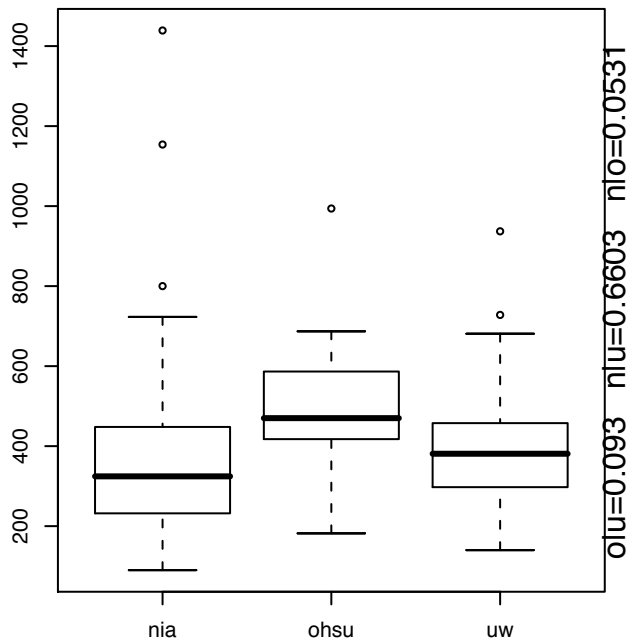
L.frontal gm mean



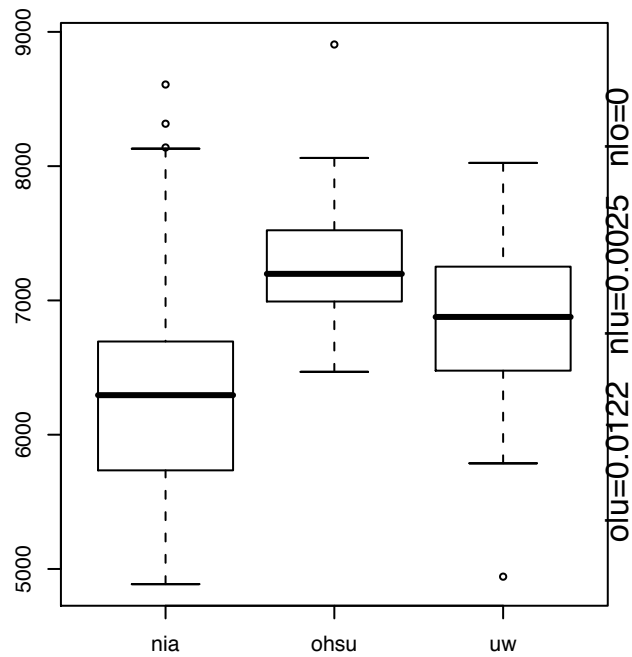
L.frontal wm mean



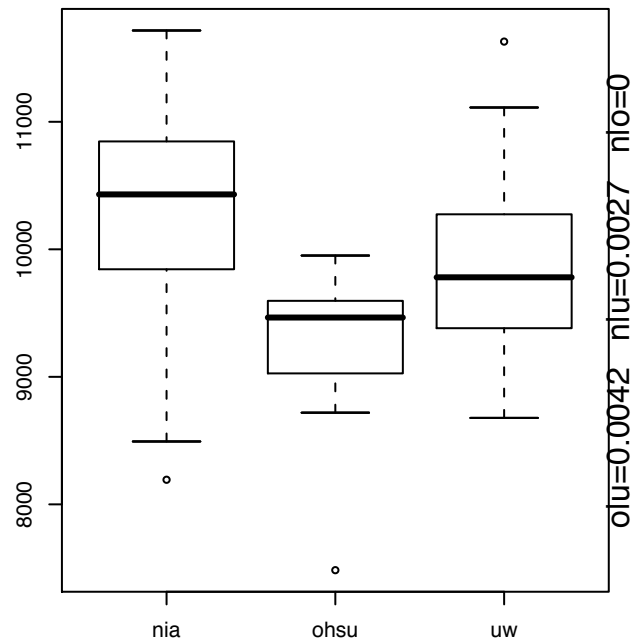
R.frontal csf voxels



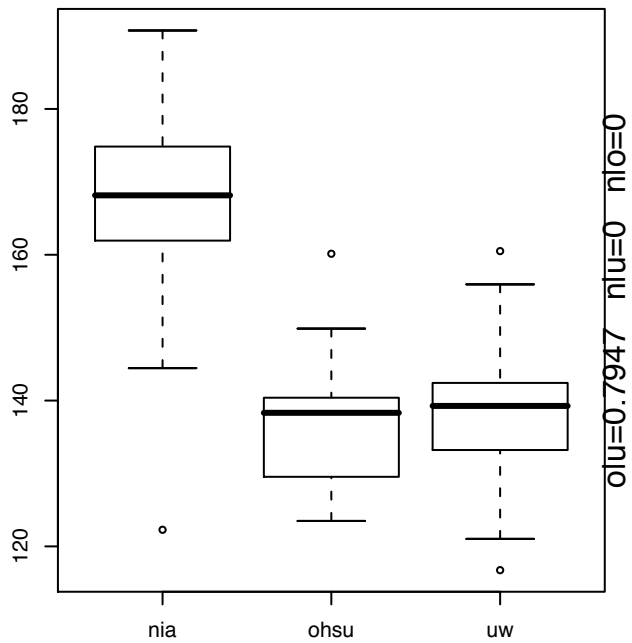
R.frontal gm voxels



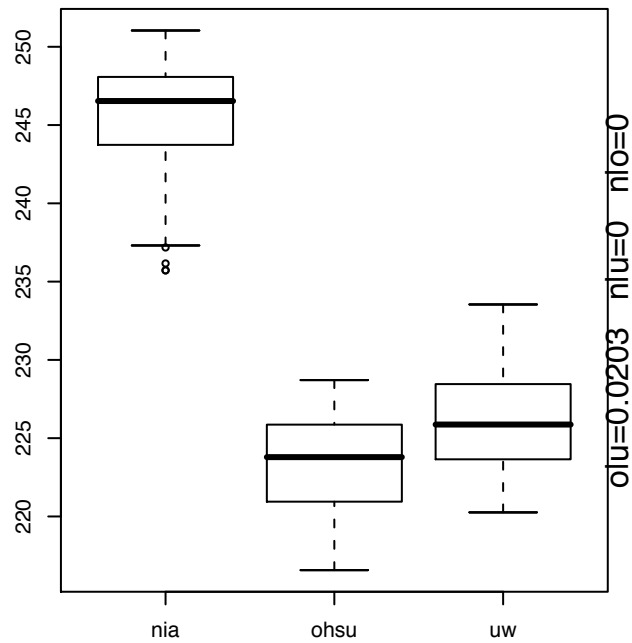
R.frontal wm voxels



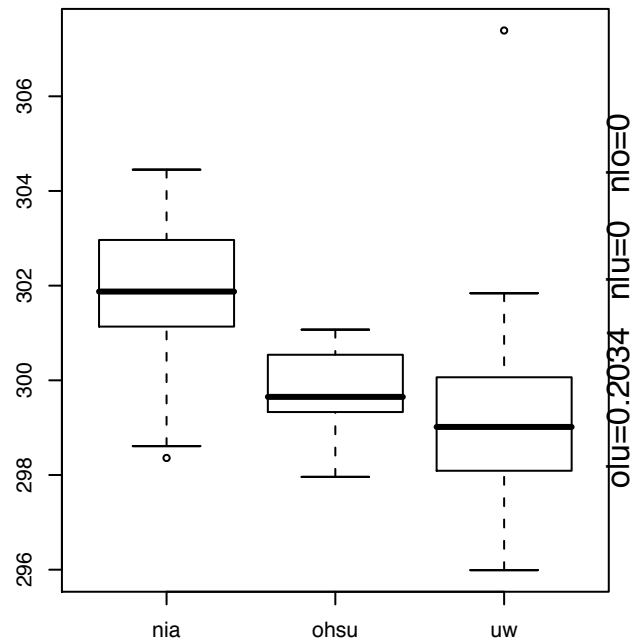
R.frontal csf mean



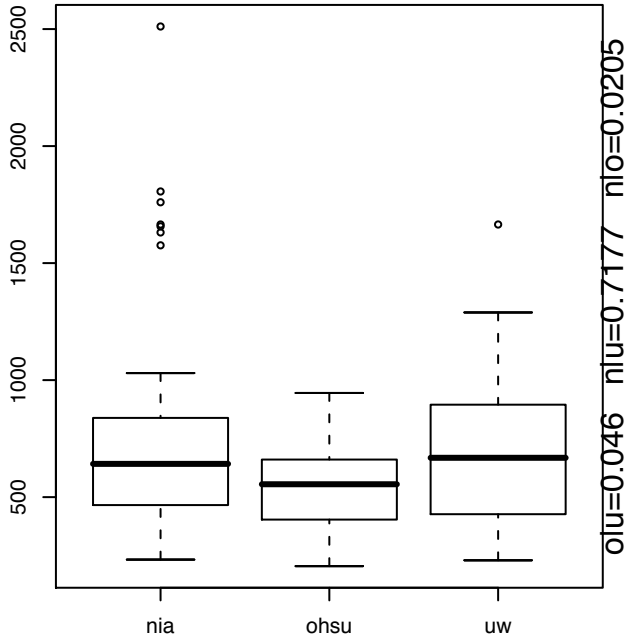
R.frontal gm mean



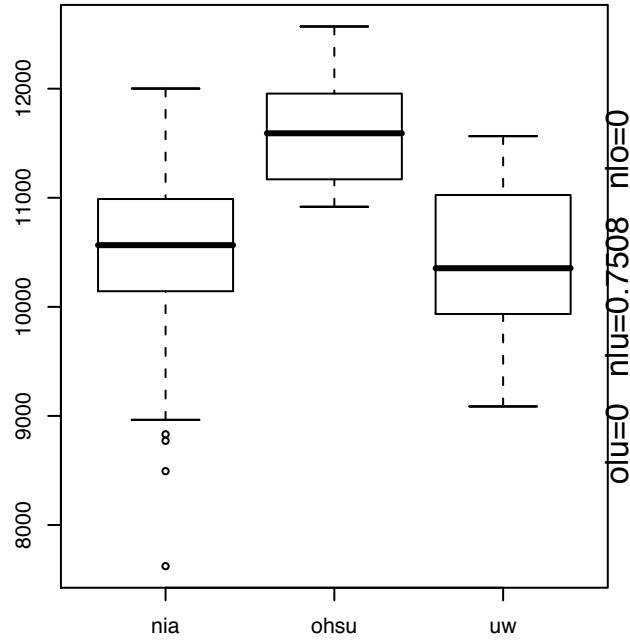
R.frontal wm mean



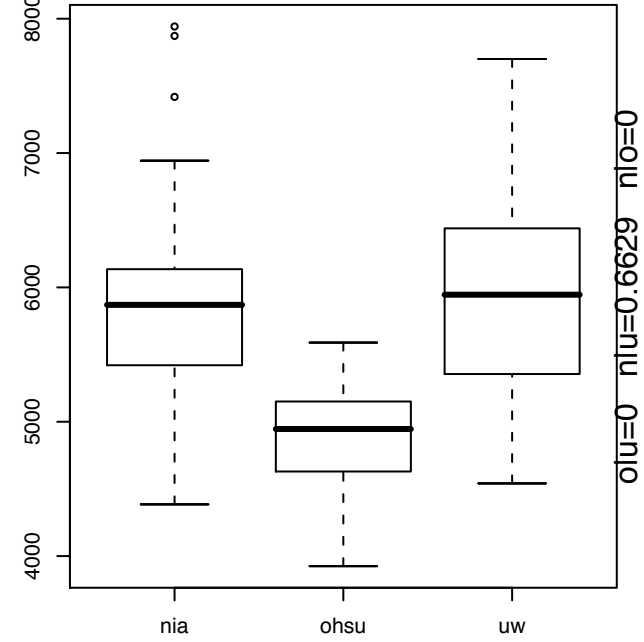
L.parietal csf voxels



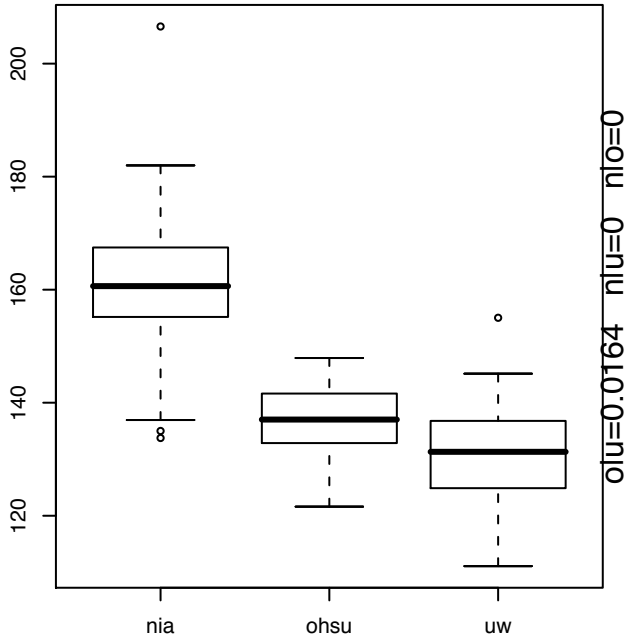
L.parietal gm voxels



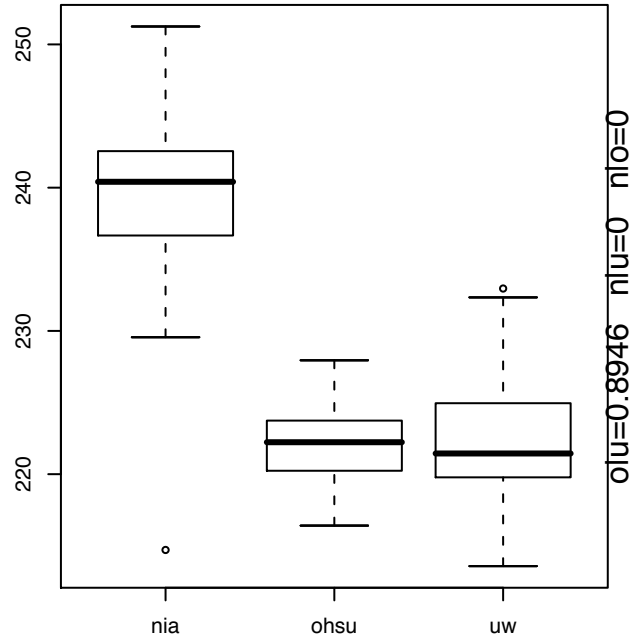
L.parietal wm voxels



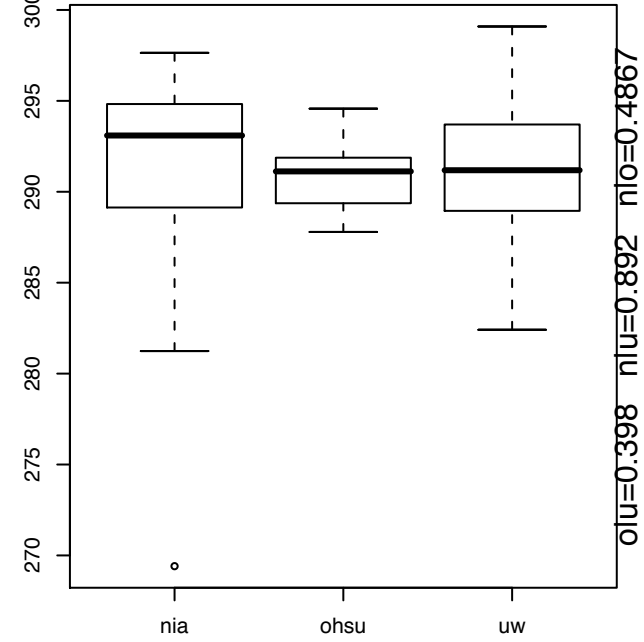
L.parietal csf mean



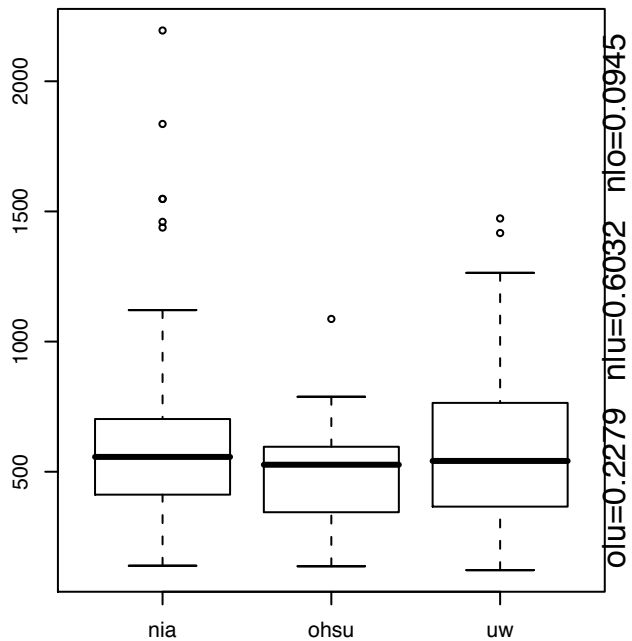
L.parietal gm mean



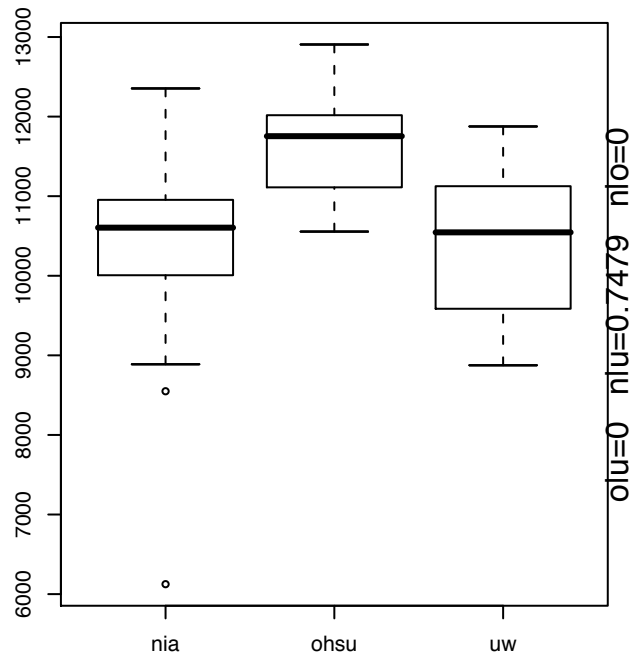
L.parietal wm mean



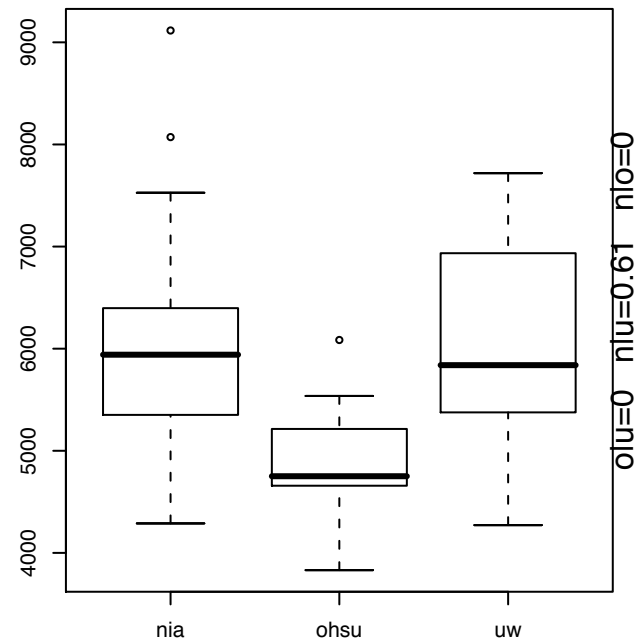
R.parietal csf voxels



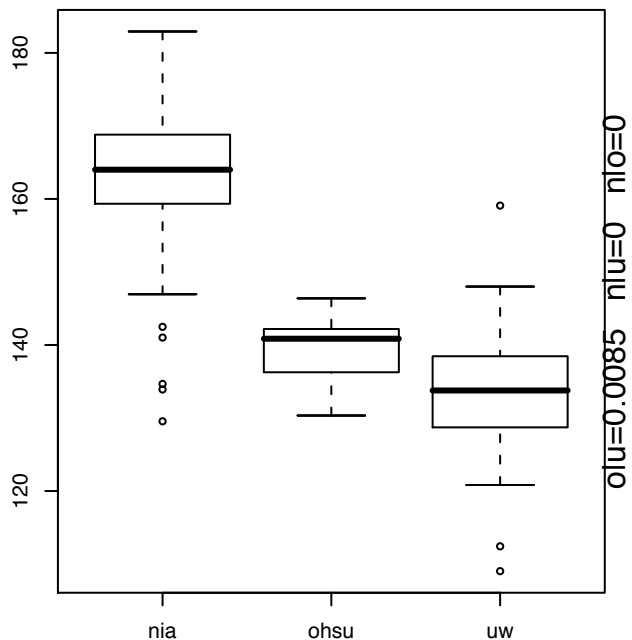
R.parietal gm voxels



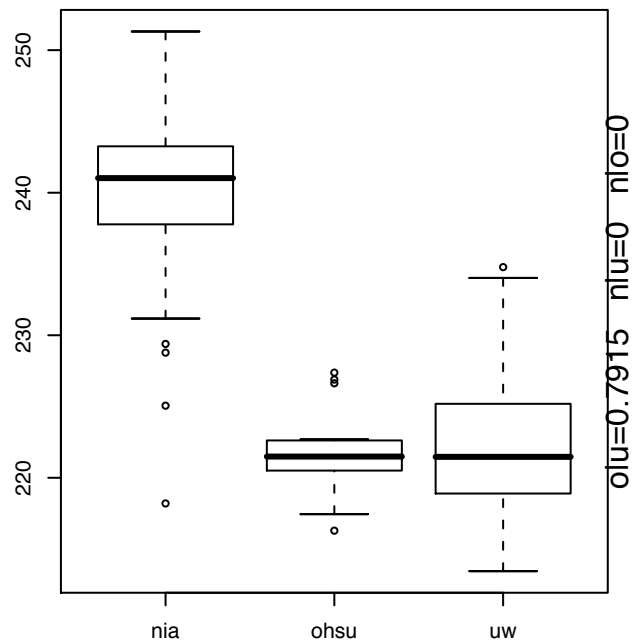
R.parietal wm voxels



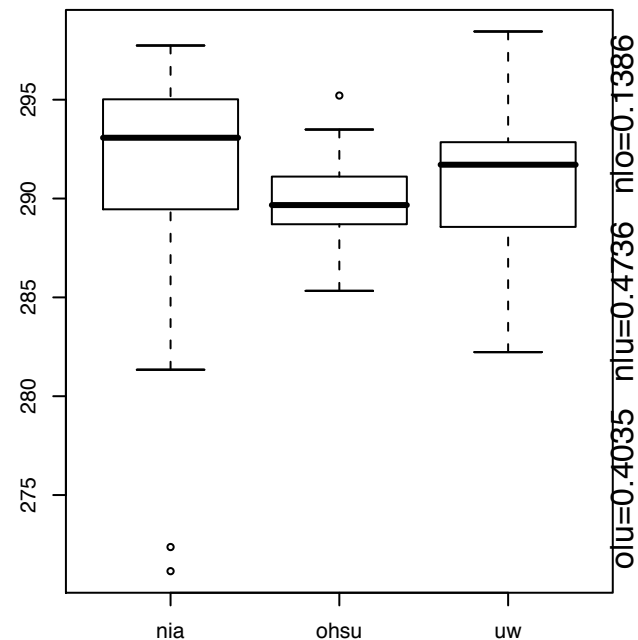
R.parietal csf mean



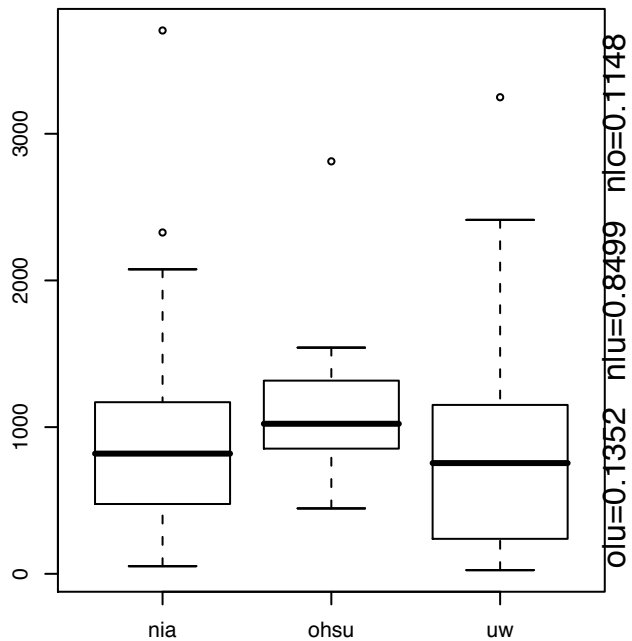
R.parietal gm mean



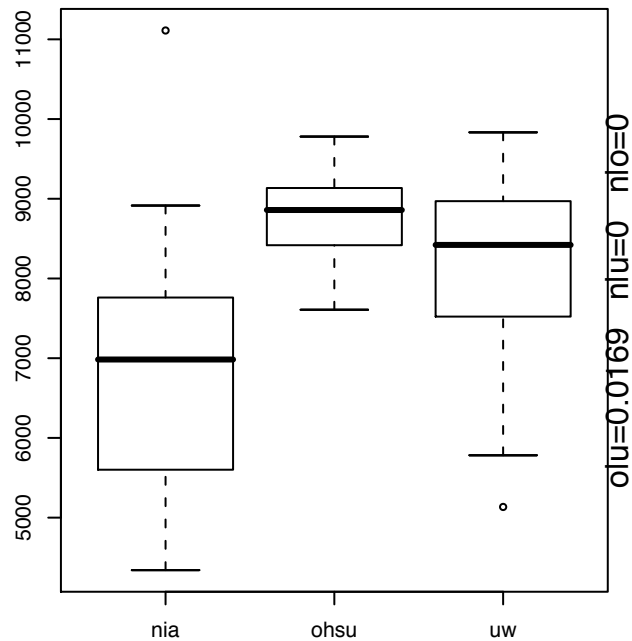
R.parietal wm mean



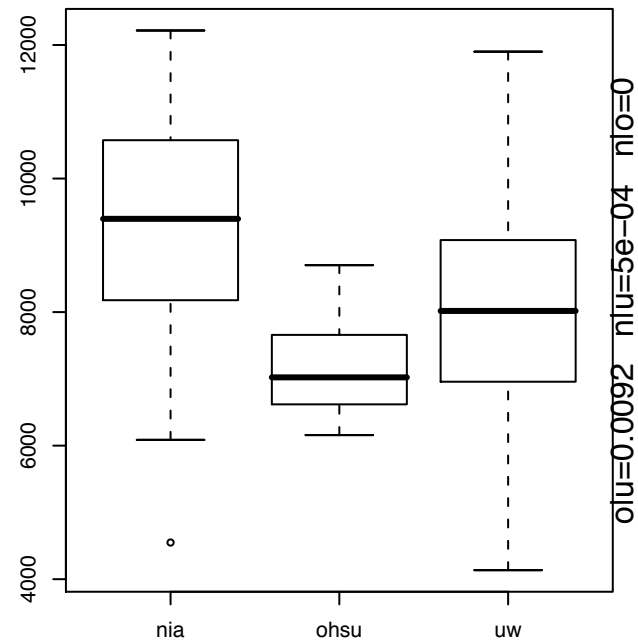
L.occipital csf voxels



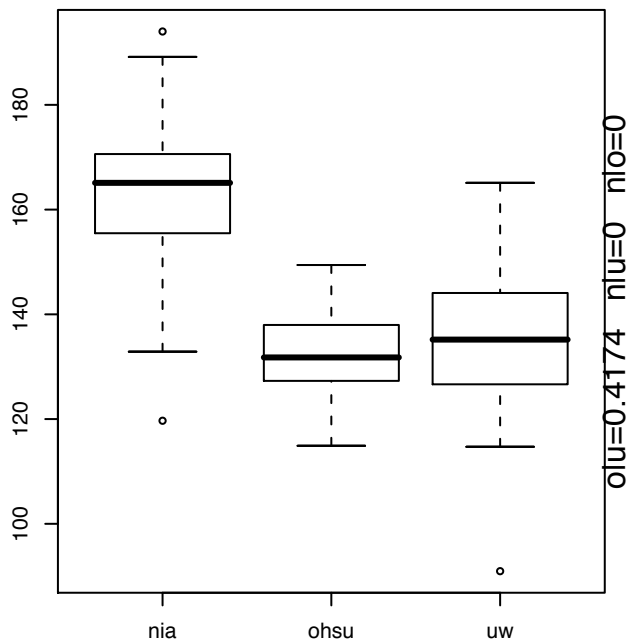
L.occipital gm voxels



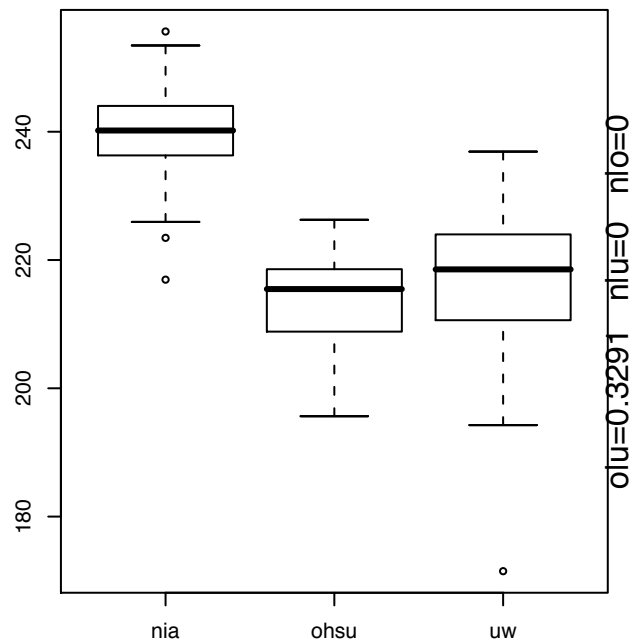
L.occipital wm voxels



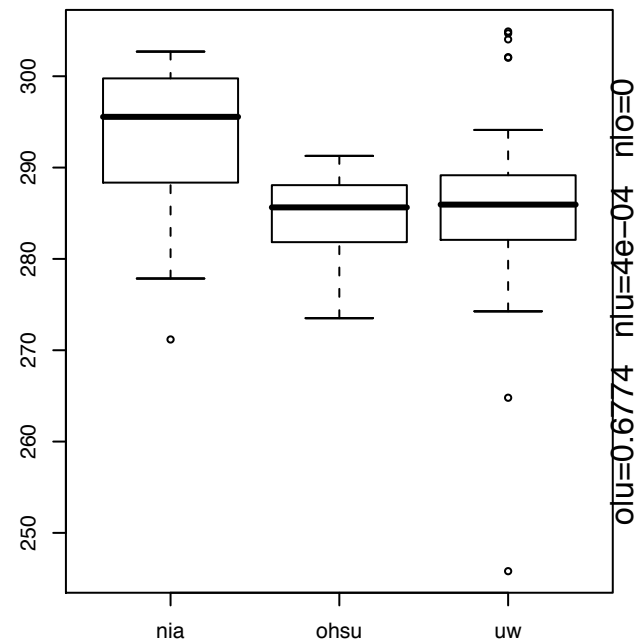
L.occipital csf mean



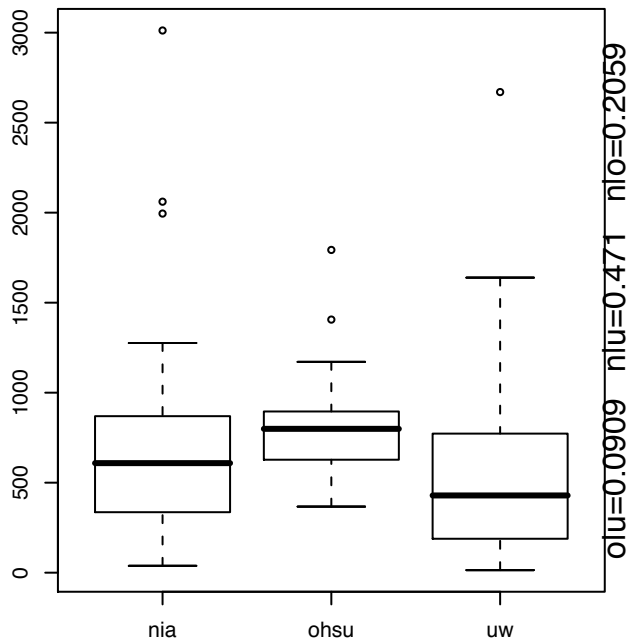
L.occipital gm mean



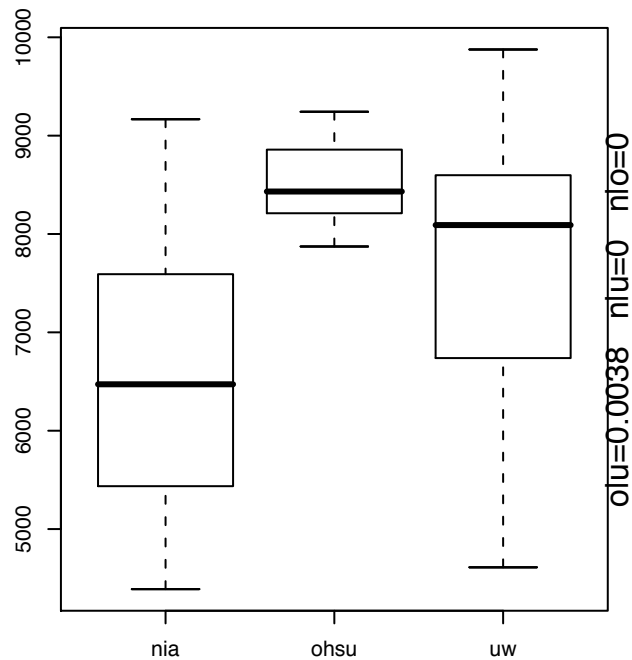
L.occipital wm mean



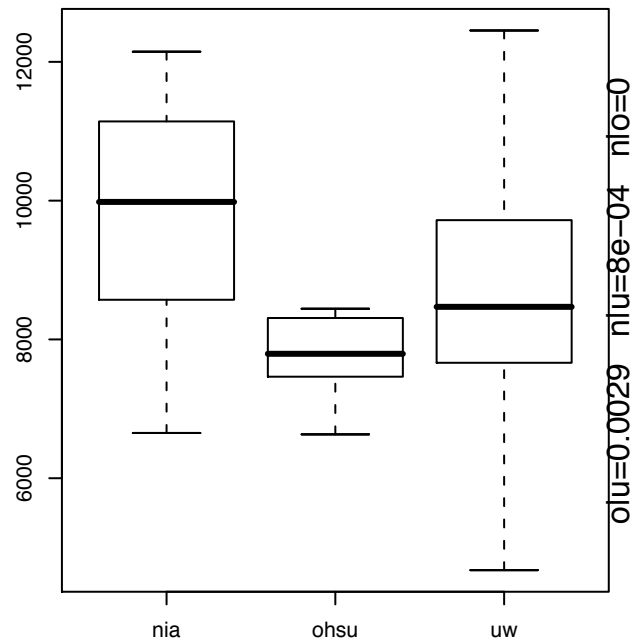
R.occipital csf voxels



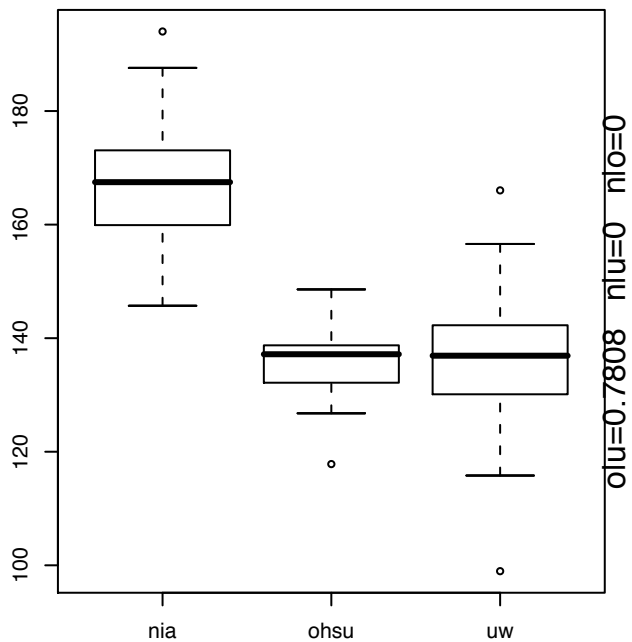
R.occipital gm voxels



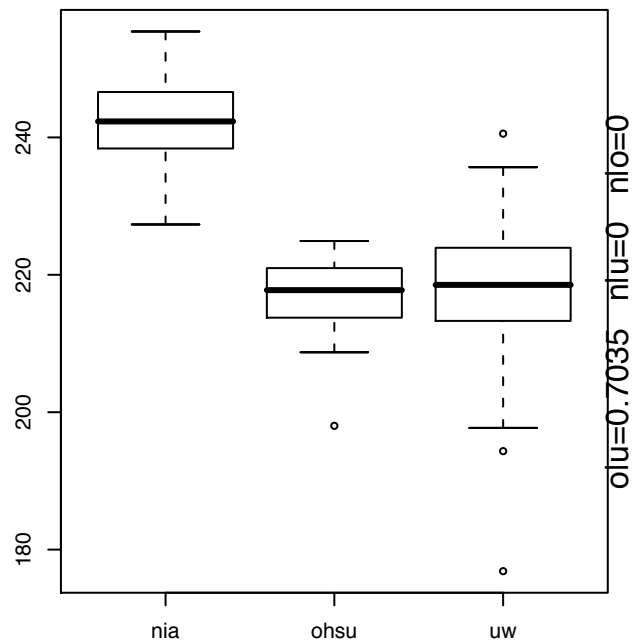
R.occipital wm voxels



R.occipital csf mean



R.occipital gm mean



R.occipital wm mean

